A prefrontal cortex-lateral hypothalamus circuit controls stress-driven food intake

L.F. Supiot[1], A.A.C. Benschop[1], A.S.J. Nicolson[1], R. Haak[1], I.G. Wolterink-Donselaar[1], M.C.M. Luijendijk[1], R.A.H Adan[1], R.B. Poorthuis[1*], F.J. Meye[1*]

1. Department of Translational Neuroscience, Brain Center, UMC Utrecht, Utrecht University, The Netherlands.

*Equal contribution / corresponding author

Abstract

Stress can drive excessive intake of palatable high-caloric food. The medial prefrontal cortex (mPFC) is implicated in this, but through unknown downstream circuits and mechanisms. Here we show, in mice, that the projection from the mPFC to the lateral hypothalamus (LHA) is a critical substrate for stress-driven fat intake. We show that optogenetic stimulation of the mPFC-LHA increases fat intake under naïve conditions. Using *in vivo* electrophysiology and ensemble tagging, we demonstrate that the mPFC-LHA network acutely responds to social stress. Combining patch clamp and optogenetics, we show that after social stress plasticity occurs specifically at mPFC synapses onto LHA glutamatergic (but not GABAergic) neurons. Such stress primes the efficacy with which optogenetic stimulation of mPFC-LHA pathways drives fat intake, while chemogenetic inhibition of this network specifically blocks stress-driven increased fat intake. Our findings identify the mPFC as a top-down regulator of distinct LHA feeding networks, necessary for stress-eating behavior.

Introduction

Stressful experiences drive excessive intake of rewarding foods rich in fat and/or sugar[1–3]. In vulnerable individuals, stress contributes to the development of obesity, or to the recurrent binge eating in Bulimia Nervosa (BN) and Binge Eating Disorder (BED)[4,5]. The prefrontal cortex (PFC), a stress-sensitive region important in decision making and strategy selection[6,7], is likely implicated in stress-driven food intake. In obese individuals and patients with BED/BN the PFC is hyperresponsive to food cues[8,9], and rodent studies have also demonstrated that stimulation of subsets of medial (m)PFC neurons can cause voracious food intake[3,10,11]. Despite its links to regulating eating behavior, it remains unknown whether the mPFC also transforms stressful experiences into excessive intake of palatable food, and if so through which network adaptations.

A likely downstream target of the mPFC is the lateral hypothalamic area (LHA). mPFC glutamatergic pyramidal neurons send direct projections to the LHA[12]. The LHA itself has a prominent role in food intake[13–16], and we recently showed that the LHA interacts with the midbrain to drive stress-driven food intake[3]. Notably however, the LHA is highly heterogeneous in (functional) neuronal subtypes[3,14,15,17,18]. In particular, glutamatergic LHA neurons (LHA_{VGLUT2} cells) are commonly linked to curtailing food intake[15,17], whereas GABAergic LHA neurons (LHA_{VGAT} cells) typically promote food intake[15,17,19]. It is unclear which of these distinct LHA subtypes are innervated by mPFC, and how mPFC control, potentially over distinct LHA cell types, orchestrates (stress-driven) feeding responses.

We hypothesized that stress would alter mPFC control over LHA networks, to causally drive excessive palatable food intake. Here we show, in mice, that optogenetic stimulation of the mPFC-LHA pathway is capable of driving specific intake of fat over chow. We use *in vivo* electrophysiology to demonstrate that mPFC cells projecting to the LHA are directly sensitive to social stress. Combining patch clamp, optogenetics and ensemble tagging, we show that mPFC cells synapse onto multiple LHA cellular subtypes, but that particularly the mPFC projections to LHA glutamatergic cells are directly engaged during acute stress (when the drive for food intake

is temporarily reduced). On the contrary, in the aftermath of stress, when the drive for food intake is increased (hyperphagia), a predominant weakening of mPFC glutamatergic synapses onto these LHA glutamate cells is observed. Using *in vivo* optogenetics and chemogenetics we show that these stress-driven circuit modifications prime the efficacy with which the mPFC-LHA network can drive fat intake, and we show that mPFC-LHA network activity after stress is indispensable for stress-eating responses. Overall we identify the mPFC as a direct regulator of LHA feeding networks, with a critical role in stress-driven food intake.

Results

mPFC-LHA stimulation, in a frequency-dependent manner, increases palatable food intake

We first assessed whether the mPFC-LHA pathway is actually capable of driving intake of palatable food, as thus far this had not been reported. Instead, prior studies evaluating the mPFC-LHA pathway showed that high frequency optogenetic stimulation (100Hz bursts) does not affect regular food intake[20], while continuous chemogenetic stimulation (or 20Hz optogenetic stimulation) decreases chow intake[21]. Notably, neural circuits of mPFC and LHA are individually known to have frequency-dependent functions[19,22]. For instance, optogenetic stimulation of LHA_{VGAT} neuronal subtypes efficiently drives food intake at specifically 5Hz, more so than at lower or higher frequencies[19]. Therefore, we first tested whether low frequency stimulation of the mPFC-LHA pathway is capable of increasing palatable food intake. We stereotactically injected C57B6 mice in the mPFC with an AAV to express the optogenetic construct CoChR (rAAV5-Syn-CoChR-GFP) or YFP control vector (rAAV5-Syn-eYFP), and targeted optic fibers to the LHA to optogenetically stimulate the mPFC-LHA pathway (Fig 1A-B; Suppl Fig. 1A). After recovery, mice were placed in a 2-choice food-context containing regular chow and fat as a palatable food source. Baseline food intake was established over 3 consecutive days, followed by a session during which the mPFC-LHA pathway was stimulated at a specific frequency (Fig. 1C). We observed that during sessions of 5Hz stimulation, but not of 1 or 10Hz,

83 there was an overall increase of fat intake (Fig. 1D). This intake was specific to fat, as it did not
84 occur for chow (Suppl Fig. 1B).

85

86 We then used video-based analysis to examine the feeding behavior within mPFC-LHA
87 stimulation blocks (ON), contrasting them with behavior during alternating non-stimulated
88 blocks (OFF). We observed that with 5Hz stimulation mice spent more time in specifically the fat
89 zone (Suppl. Fig. 1C). Furthermore, we observed that the effect of pathway stimulation on fat
90 consumption was differed over the course of the task. Interactions with fat normally waned
91 over the hour (Fig. 1E). Whereas 5Hz stimulation of the pathway did not affect fat intake at the
92 start when the drive for fat was still high, it instead drove continued fat consumption later on
93 when such interactions waned in control groups or in 1Hz stimulation conditions (Fig. 1E).
94 Consequently, 5Hz stimulation resulted in overall more feeding bouts for fat, but not chow (Fig.
95 1F; Suppl. Fig. 1D). These effects on food intake did not stem from effects of pathway
96 stimulation on general locomotor activity (which increased linearly in a different pattern from
97 the effect on food intake; Suppl. Fig. 1E), nor did they stem from any direct alterations of
98 emotional valence states, as assessed with a real-time place preference/avoidance assay (Suppl.
99 Fig. 1F). Overall these data indicate that the mPFC-LHA pathway is able, in the lower frequency
100 domain, to drive the continued intake of palatable fat.

101

102 **mPFC cells projecting to LHA directly modulate their firing in response to an acute social**
103 **stressor that causes hypophagia.**

104 Stressful experiences can have strong bidirectional effects on food intake[23]. Immediately during
105 a stress experience (i.e. acute stress) a transient reduction occurs in food intake (i.e.
106 hypophagia). Instead, in the hours to weeks after the stress, excessive food intake can occur (i.e.
107 hyperphagia)[3,24], ultimately causing weight gain[24]. We reasoned that if the mPFC-LHA network
108 would be involved in stress-driven effects on food intake, that it should be able to detect
109 stressful information. To test this hypothesis, we used a social stress experience, where a mouse
110 is temporarily exposed to the aggression and proximity of a dominant conspecific. This

111 naturalistic stress experience is capable of inducing separable states of hypo- and hyperphagia.
112 We and others have previously shown that hours to days after the social stress, increased intake
113 of fat occurs (hyperphagia)[3,24]. Conversely, we confirmed that immediately after such a social
114 stress episode (i.e. the first hour after it ends), there is a suppressed intake of palatable fat (i.e.
115 hypophagia; Suppl. Fig. 2A-B).

116 We assessed whether social stress would immediately engage the mPFC-LHA pathway. To this
117 end we performed *in vivo* electrophysiological recordings from mPFC cells projecting to the LHA.
118 We injected, in C57B6 mice, a canine adeno virus in the LHA to retrogradely deliver cre (Cav2-
119 Cre) to the mPFC, and an AAV in the mPFC to cre-dependently drive an opsin (AAV-DIO-
120 hChR2(H134R)-mCherry). We then chronically implanted electrodes together with an optic fiber
121 (i.e. an optrode) in the mPFC of these mice (Fig. 2A-B). This allowed for optogenetic-assisted
122 identification (i.e. opto-tagging) of mPFC cells that projected to the LHA (Fig. 2C; Suppl. Fig. 2C-
123 D). We then exposed these mice to the sensory proximity of a CD1 mouse and the actual fight
124 experience with such an aggressor, while performing single cell recordings from opto-tagged
125 mPFC-LHA cells (Fig. 2D). We analysed firing rates of opto-tagged neurons before, during and
126 after the period in which fighting took place. Divergent responses were observed in mPFC
127 neurons projecting to LHA during stress, with approximately half of the cells decreasing their
128 firing rates during fight periods, whereas others instead increased their firing rates (Fig. 2E-F).
129 These effects were not solely linked to the physical altercation, as they outlasted the fighting
130 period (Fig. 2E; Suppl. Fig. 2E). In further support of this, we also evaluated the responses of
131 these same neurons when the CD1 mouse arrived in the cage, while still behind a semi-
132 permeable barrier (i.e. sensory stress). We observed similar response types, where in particular
133 the neurons that increased their firing during physical exposure, were also recruited during such
134 sensory stress (Suppl. Fig. 2F-I). Overall, these data suggest the existence of different
135 populations of mPFC-LHA neurons, with certain mPFC-LHA neurons acutely decreasing their
136 activity, and others directly increasing it upon social stress exposure. These findings confirm the
137 hypothesis that mPFC cells that project to LHA are directly able to detect a social stressor with
138 both short-term hypophagic and longer-term hyperphagic properties.

139

140

141

142 **mPFC connects to multiple LHA neuronal populations, but during an acute social stress**
143 **causing hypophagia stress-activated mPFC neurons preferentially target LHA glutamatergic**
144 **subsets.**

145 Our findings demonstrate that the mPFC neurons projecting to the LHA are capable of altering
146 food intake, and are acutely reactive during stress. However, it is unclear which LHA neuronal
147 subtypes are innervated by the mPFC. The LHA contains both glutamatergic populations,
148 expressing the vesicular glutamate transporter 2 (LHA_{VGLUT2}) and GABAergic populations,
149 identified by expression of the vesicular GABA transporter (LHA_{VGAT}). Recent transcriptomic
150 evidence suggests that essentially all LHA neurons can be ascribed to one of these major classes,
151 with further key subpopulations occurring within them[15,18]. For instance, evidence suggests that
152 orexin (LHA_{OREX}) and melanin-concentrating hormone (LHA_{MCH}) releasing neurons represent
153 subsets of LHA glutamatergic neurons[18]. We reasoned that, despite further heterogeneity within
154 LHA_{VGLUT2}, LHA_{VGAT}, LHA_{MCH} and LHA_{OREX} neuronal sets[15,18], these four populations offer a starting
155 point to understand mPFC functional innervation patterns of the LHA.

156 To map mPFC connectivity to these four LHA subpopulations we performed an optogenetic-
157 assisted synaptic connectivity study[25,26]. We targeted the mPFC with the opsin CoChR (AAV5-
158 Syn-CoChR-GFP) and fluorescently labeled LHA_{VGLUT2}, LHA_{VGAT}, LHA_{MCH} or LHA_{OREX} populations
159 with viral and transgenic strategies. For LHA_{VGLUT2} and LHA_{VGAT}, populations we used well-
160 established transgenic mice VGLUT2-Cre or VGAT-Cre mice, respectively (Fig. 3A-B). We injected
161 these mice in the LHA with an AAV to cre-dependently express a red fluorophore (rAAV-EF1a-
162 DIO-mCherry) to label either LHA_{VGLUT2} or LHA_{VGAT} neurons, respectively (Fig. 3A-B). Instead to
163 target LHA_{OREX} or LHA_{MCH} neurons we injected C57B6 mice with an AAV to drive expression of a
164 red fluorophore under the control of short promotors for either MCH (AAV-MCHpr-Gq-mCherry)
165 or orexin (AAV-hORXpr-dTomato)[27] (Fig. 3A-B). We established the specificity of this approach
166 using post-hoc labeling of biocytin-filled patched cells expressing either the fluorophore under
167 control of the orexin or the MCH promotor (Suppl. Fig. 3A-C). We also established that the
168 LHA_{VGLUT2} cells that we on average targeted were distinct from the LHA_{OREX} and LHA_{MCH} cells, as

169 those peptidergic subpopulations of glutamatergic neurons differed strongly in somatic cell size
170 from typical LHA_{VGLUT2} neurons (Suppl. Fig. 3D). We then performed *ex vivo* patch clamp
171 recordings to assess the occurrence of mPFC synaptic inputs onto these LHA subpopulations.
172 We observed high degrees (≥80%) of connectivity between mPFC cells and all four LHA
173 populations (Fig. 3C). We then repeated these experiments in the presence of a
174 pharmacological cocktail of tetrodotoxin (TTX) and 4-aminopyridine (4-AP) in the external
175 medium[25,28] and confirmed that the high extent of connectivity of mPFC inputs with all LHA
176 subtypes was due to direct monosynaptic connections (Fig. 3D). We then further characterized
177 the properties of LHA cells with confirmed mPFC synaptic inputs. First, we established that the
178 different LHA neuronal populations could be driven to fire action potentials in response to mPFC
179 stimulation (Suppl. Fig. 3E). Then, we determined the specific excitability profiles of these mPFC-
180 innervated LHA cell types. Notably, LHA_{VGAT} neurons were more excitable than the other
181 populations, particularly at relatively lower current inputs (Suppl. Fig. 3F-J). Together these data
182 indicate that there is a strong monosynaptic projection from the mPFC cells to all four LHA
183 subpopulations, and that of all these mPFC-innervated LHA targets, the LHA_{VGAT} cells present the
184 highest excitability with low stimulation.

185

186 These data show that mPFC cells can innervate multiple LHA subtypes. During acute stress,
187 when there is a hypophagic response (Suppl. Fig. 2A-B), we showed that some mPFC neurons
188 projecting to LHA show increased firing during this period (Fig. 2E-F). Therefore, we asked
189 whether particular branches of the mPFC-LHA multiform network would be preferentially
190 engaged during such a hypophagic state. These could be, for instance, LHA neurons with general
191 roles in curtailing food intake, like LHA_{VGLUT2} neurons[15,17]. To address this we expressed an
192 optogenetic construct in those mPFC cells that were reactive during the acute social stress (as
193 opposed to all mPFC neurons). To that end we used TRAP2 (Targeted Recombination in Active
194 Populations) transgenic mice, in which the immediate early gene c-Fos can drive Cre-ERT2
195 expression, which can then be conditionally transported from the cytosol to the nucleus in a
196 manner dependent on 4-OH tamoxifen[29]. We previously showed that this strategy can be
197 leveraged to capture social stress-reactive neuronal ensembles[30]. We crossed these TRAP2

198 transgenic mice with either VGAT-Cre or Vglut2-Cre mice and used the resultant offspring. We
199 first injected an AAV driving cre-dependent CoChr in the mPFC and exposed the mice to two
200 acute stress episodes, where each episode was paired with a 4-OH tamoxifen injection. Weeks
201 later we also injected AAVs in the LHA to fluorescently label specific subpopulations such as
202 $LHA_{VGLUT2,}$ LHA_{VGAT}, LHA_{OREX} and LHA_{MCH} cells as before (Fig. 3A-B, E). Importantly, while both
203 TRAP2 transgenic mice, and VGAT-Cre / VGLUT2-Cre transgenic mice, rely on conditional
204 expression via the same Cre-LoxP system, the viral injection scheme in this case avoided
205 interference between this. First, we avoided mPFC CoChR expression in a manner not linked to
206 the TRAPing of an ensemble in the VGLUT2-Cre mice, on the basis of mPFC neurons expressing
207 VGLUT1 rather than VGLUT2[21,31] (Suppl. Fig. 3K). We also avoided that there would be Cre-
208 dependent fluorophore recombination in the LHA driven by the TRAP system rather than on the
209 basis of LHA cell type identity, by performing the LHA viral injection several weeks after the
210 4OH-tamoxifen dependent TRAPing event in the mPFC had taken place (Fig. 3E), whereas the
211 time window in which 4OHT allows Cre to travel to the nucleus for recombination is only a
212 matter of hours[29,30]. Finally, we also took along a control ensemble of exposure to a novel
213 mouse rather than stressful altercations (Fig. 3E). In both the social stress TRAP experiment and
214 the novel mouse TRAP experiment we observed expression of CoChR in mPFC ensembles (Fig.
215 3F; Suppl. Fig. 3L). We then performed patch-clamp recordings in the LHA, and assessed
216 whether optogenetic stimulation of $mPFC_{NOVEL\ MOUSE}$ or $mPFC_{SOCIAL\ STRESS}$ ensembles resulted in
217 synaptic contacts with specific LHA cell types. Stimulating the $mPFC_{NOVEL\ MOUSE}$ ensemble caused
218 little to no synaptic connectivity with any of the LHA cell types (Fig. 3G). In contrast,
219 optogenetically stimulating the $mPFC_{SOCIAL\ STRESS}$ ensemble resulted in synaptic responses in
220 LHA_{VGLUT2}, LHA_{MCH}, and LHA_{OREX} neuronal subsets (Fig. 3G). Instead, LHA_{VGAT} neurons received
221 almost no input (Fig. 3G).

222

223 Overall, our data suggest that the mPFC forms a functional network with four distinct LHA
224 subpopulations, but that during acute social stress (coinciding with hypophagic states), an mPFC
225 ensemble of neurons is engaged that selectively targets LHA glutamatergic subtypes, of which

226 LHA_{VGLUT2} cells are commonly linked to curtailing food intake[15,17], over LHA_{VGAT} cells whose
227 activity typically promotes food intake[15,17,19].

228

229

230 **Under subsequent stress-driven hyperphagic conditions, there is reduced mPFC synaptic**
231 **strength specifically onto LHA_{VGLUT2} neurons via presynaptic processes.**

232 After the acute hypophagic effects of social stress (Suppl Fig. 2A-B), there is an opposite and
233 more durable hyperphagic intake of palatable food sources rich in sugar and fat[3,24], which
234 ultimately results in excess body weight if maintained over weeks[24]. We next asked if, at the
235 time of stress-driven hyperphagia, mPFC synaptic strength onto distinct LHA neuronal
236 populations would be altered. Such protracted plasticity effects could occur in specifically the
237 $mPFC_{ACUTE\ STRESS}$ ensemble, but could also occur in other mPFC cells. Therefore, we again
238 evaluated (all) mPFC synaptic contacts onto the four distinct LHA populations (LHA_{VGLUT2},
239 LHA_{VGAT}, LHA_{MCH}, LHA_{OREX}). We expressed an opsin in the mPFC (AAV-CoChR-GFP) and tagged
240 distinct LHA populations as before (Fig. 3A-B; Fig. 4A-B). We exposed mice to two days of
241 control experience or social stress, and then the next day, when mice normally engage in higher
242 intake of palatable food[3], we made brain slices and assessed synaptic properties at mPFC
243 synapses onto the four broad classes of LHA neuronal populations (Fig. 4A-B).

244

245 Interestingly, we observed that specifically at the mPFC synapses onto LHA_{VGLUT2} neuronsthere
246 was a stress-induced decrease in maximally optogenetically-evoked EPSC magnitudes (Fig 4C-E;
247 Suppl. Fig 4A). This suggests a weakening of $mPFC_{GLU}$ synapses onto LHA_{VGLUT2} neurons. To
248 further address the underlying mechanisms for this we assessed the paired pulse ratio (PPR), a
249 measure inversely related to presynaptic release probability[25]. We observed that specifically at
250 mPFC- LHA_{VGLUT2} synapses there was an increased PPR, in accordance with a scenario of lower
251 release probability at these synapses due to prior social stress (Fig. 4F-H; Suppl. Fig. 4B). The
252 effect of stress was specific to the presynaptic compartment, as we did not observe a difference
253 in postsynaptic glutamatergic receptor distributions at these synapses (Suppl. Fig. 4C-F). Nor did

254 we observe changes due to stress in terms of the excitability of the LHA cells or in basic
255 membrane properties (Suppl. Fig. 4G-N). Overall, these data suggest that a day after a social
256 stress experience, at a moment where animals are inclined to binge on fat[3], there is a
257 weakening of mPFC glutamatergic synapses onto LHA_{VGLUT2} neurons, which upon activation
258 would typically reduce food intake[15,17].
259
260 **Social stress has divergent effects on distinct populations of mPFC-innervated LHA_{VGLUT2} cells**
261 LHA_{VGLUT2} neurons still represent a very heterogeneous population[18] and in part this
262 heterogeneity is reflected by their distinct projection targets[32]. For instance, stimulating
263 LHA_{VGLUT2} projections to the lateral habenula (LHb) suppresses food intake[33]. Similarly
264 stimulating LHA_{VGLUT2} neuronal projections to midline hypothalamic regions around the third
265 ventricle (i.e. peri-paraventricular nucleus, or peri-PVN region[34]) is linked to aversive processes[35]
266 and reduced food intake[36]. Instead LHA_{VGLUT2} projections to the ventral tegmental area (VTA) do
267 not alter food intake under naïve conditions[3,37,38], but the potentiation of their synapses onto
268 dopamine neurons causally contributes to the enhanced fat intake occurring after social stress[3].
269 Given this LHA_{VGLUT2} anatomical but also functional divergence, we therefore asked how social
270 stress would affect mPFC synapses onto such distinct LHA_{VGLUT2} populations. We first confirmed
271 that the LHb, VTA and (peri)-PVN were likely downstream targets of mPFC-innervated LHA
272 neurons. For this we used a transsynaptic tracing strategy (Suppl. Fig. 5A) in which we injected
273 AAV1-Cre in the mPFC, to cause a transsynaptic jump to downstream neurons[39]. We then
274 injected an AAV-DIO-GFP in the LHA to perform anterograde tracing of the nerve terminals
275 belonging to LHA neurons with mPFC-innervation (Suppl. Fig. 5A-C). We indeed observed
276 anterograde terminals in the aforementioned regions of interest like the VTA, the LHb and the
277 peri-PVN (Suppl. Fig. 5D-F).
278
279 We then investigated if and what type of stress-driven synaptic changes occurred at mPFC
280 synapses onto LHA_{VGLUT2} neurons projecting to LHb, VTA and peri-PVN. To label LHA_{VGLUT2} cell
281 types based on their projection output, we injected a Cre-dependent retrograde tracer
282 (retroAAV-DIO-mCherry) in Vglut2-cre mice in these three different areas (Fig. 4I). We then

283 again exposed mice to either two days of control or social stress conditions and we prepared
284 brain slices the day after (Fig. 4I). We observed that mPFC synapses onto LHA_{VGLUT2}-Peri-PVN
285 neurons exhibited higher PPR upon stress (Fig. 4J), in accordance with the general effect of
286 stress on the LHA_{VGLUT2} neurons (Fig. 4F). Interestingly, mPFC synapses onto LHA_{VGLUT2}-VTA
287 neurons presented a lower PPR after stress, suggesting enhanced release probability of mPFC
288 synapses onto those specific LHA_{VGLUT2} neurons (Supp. Fig. 5G), while we did not observe PPR
289 changes at mPFC synapses onto LHA_{VGLUT2}-LHb neurons after stress (Supp. Fig. 5H).
290
291 Overall, these data suggest that social stress has divergent effects on the strength of mPFC
292 synapses onto distinct LHA_{VGLUT2} populations. At a time point where stress drives
293 overconsumption of fat, there is strengthening of the excitatory mPFC synapses onto LHA_{VGLUT2}
294 projections to the VTA in the midbrain: a downstream circuit for which we previously showed
295 that also strengthening of LHA glutamatergic synapses onto VTA dopamine neurons is linked to
296 stress-driven fat intake[3]. However, it is likely that these LHA_{VGLUT2} projections to the VTA are a
297 relative minority amidst other LHA_{VGLUT2} neurons, as the effect of stress on mPFC synapses onto
298 the general population of LHA_{VGLUT2} neurons was a reduction in synaptic strength. We show that
299 amongst the LHA_{VGLUT2} populations for which this is the case, are those that project to the peri-
300 PVN, a region for which the activity is indeed linked to suppressing food intake and promoting
301 defensive responses[35,36].
302
303 **After social stress *in vivo* mPFC-LHA stimulation drives fat intake to an even greater extent, by**
304 **preventing a decline of interest in fat.**
305 We thus far showed that the mPFC-LHA pathway comprises multiple branches and that social
306 stress drives divergent synaptic adaptations in some of these, consistent with weakened brakes,
307 and potentially also strengthened drives, towards palatable food intake. We reasoned that the
308 consequences of such stress-driven network modifications could prime the mPFC-LHA pathway
309 to become even more capable of driving palatable food intake when stimulated. We therefore
310 predicted that 5Hz stimulation of the mPFC-LHA circuit (e.g. as in Fig. 1D-F), after social stress-

311 driven plasticity in this network had taken place, would result in even further intake of palatable
312 food.

313 To test this, we again optogenetically probed the entire mPFC-LHA pathway, by stereotactically
314 injecting C57B6 mice with an optogenetic construct (rAAV5-Syn-CoChR-GFP) and implanting
315 optic fibers bilaterally above the LHA (Fig. 5A-B). After recovery we either exposed the mice to
316 two days of social stress or housed them with a novel cage mate. Subsequently we placed the
317 animals in a limited access food choice setting, where they could consume fat or chow for 2
318 hours. Mice were again exposed to recurring blocks of optogenetic stimulation of 5Hz, or
319 instead to mock stimulation (Fig. 5A). We observed that even though mice that had previously
320 experienced stress already consumed more fat than control mice, 5Hz stimulation could drive
321 their intake of palatable food even further, making these mice the largest consumers of fat (Fig.
322 5C), in the absence of effects on chow (Suppl. Fig. 6A).

323 The overall fat intake reflected the outcome at the end of the two hour binge period. We next
324 addressed, with more fine-grained temporal resolution, whether 5Hz stimulation was more
325 efficient in driving fat intake in stressed mice as compared to control mice. We first aimed to
326 better understand the development of fat intake under stress (without pathway stimulation).
327 We observed that regular (not stimulated) stressed animals performed over 75% of their fat
328 feeding bouts in the first 20 minutes of a session, and then strongly diminished interaction with
329 the fat from thereon (Fig. 5D-E). This binge-like feeding pattern of fat for stressed mice was
330 different from control mice, which had fewer immediate feeding bouts, but continued having
331 feeding bouts for a longer period (Fig. 5D-E). We then analyzed how in these two distinct phases
332 that we refer to as “Binge Phase” (i.e. 0-20 min) and “Post-Binge phase” (20-120 min), mPFC-
333 LHA pathway stimulation affected fat interaction. Reminiscent of our previous finding of
334 pathway stimulation early in the two choice session in naïve mice (Fig. 1E), we found that 5Hz
335 mPFC-LHA stimulation was not effective in the early “Binge Phase” of the session (Fig. 5F).
336 Instead in the subsequent “Post Binge” phase 5Hz stimulation particularly drove stressed mice
337 more potently towards the fat, when they normally would likely be in more sated conditions
338 (Fig. 5G).

339 To investigate whether indeed the 5Hz stimulation could prevent a decline of interest for the
340 fat, we plotted the relative drive for fat eating over the course of the task by comparing the
341 relative amount of feeding bouts taking place during the binge and post-binge period. Indeed,
342 particularly in stressed mice, 5Hz stimulation did not affect the binge intake, but it did
343 counteract the normally occurring decline of interest in the fat later on (Fig. 5H; Suppl. Fig. 6B).
344 Overall, these data suggest that in stressed conditions, when specific adaptations occur within
345 the multi-branched mPFC-LHA network, stimulation of this network does not perturb early
346 binge intake, and causes continued fat intake afterwards, contributing to the overall larger fat
347 intake (Fig. 5C).

348

349 ***In vivo* mPFC-LHA chemogenetic inhibition specifically reduces excess fat intake after stress.**
350 We showed that mPFC-LHA pathway stimulation leads to an increased drive for palatable food
351 intake and that stress primes the pathway to enhance food intake even further. Next, we
352 addressed whether the mPFC-LHA pathway is necessary for stress-driven food intake and/or for
353 other types of food intake. For that we performed chemogenetic inhibition experiments when
354 mice were either consuming fat under regular conditions (no stress), or under hypophagic
355 conditions (during acute stress) or under hyperphagic conditions (in the aftermath of social
356 stress). For this we bilaterally expressed an inhibitory chemogenetic receptor in the mPFC-LHA
357 pathway in C57B6 mice. Specifically, we stereotactically injected Cav2-Cre retrograde virus in
358 the LHA, and an AAV to Cre-dependently drive hM4Di in the mPFC (Fig. 6A-B; Suppl. Fig. 7A).
359 Interestingly, while inhibiting the pathway had no effect on food intake for non-stressed mice, it
360 could completely counteract overconsumption of palatable food intake in stressed mice (Fig. 6C,
361 Suppl. Fig. 7B). No differences were observed for chow intake (Fig. 6C). These data suggest that
362 within the mPFC-LHA pathway there are at least certain (sub)branches for which the ongoing
363 activity is critical to drive overconsumption of fat after a stressful experience. mPFC-LHA
364 pathway inhibition did not affect locomotor behavior in the 2-choice food paradigm (Suppl. Fig.
365 7C), nor did it affect measures for locomotor activity or for anxiety in the open field test (Suppl.
366 Fig. 7D-E). To investigate whether the involvement of the mPFC-LHA pathway extends to acute
367 stress, where stress leads to hypophagic responses (Suppl. Fig. 2A-B), we exposed the mice to

368 acute social stress and put them in the food context immediately 15 min later. Prior mPFC-LHA
369 pathway inhibition did however not prevent hypophagic responses after acute stress (Fig. 6D;
370 Suppl. Fig. 7F).

371 Together these data reveal that mPFC-LHA pathway is necessary to drive hyperphagic responses
372 after repeated social stress, but is not necessary to drive acute temporary hypophagia during
373 the social stress experience.

374 **Discussion**

375 The neurobiological underpinnings of stress-driven overconsumption of palatable foods are an
376 important topic, also in view of the contributions of such behavior to disorders like Binge Eating
377 Disorder and Bulimia Nervosa, and to obesity[2,40]. The prefrontal cortex is implicated in binge
378 eating disorders[9], but it has been unclear through which network adaptations it could
379 orchestrate stress-driven food intake. Here we show that there is direct mPFC control over
380 distinct LHA circuits, and that the mPFC-LHA connections specifically contribute to stress-driven
381 overconsumption of fat, but not to regular fat intake under non-stressed conditions.

382

383 <u>The mPFC-LHA pathway has a conditional role in regulating food intake</u>

384 We propose that the connections between the mPFC and LHA do not encode a singular function
385 with regards to food intake, but are rather able to either increase or decrease it, depending on
386 the context. Prior studies showed that chemogenetic or high frequency optogenetic stimulation
387 of the $mPFC_{VGLUT1}$-LHA pathway reduced intake of chow in mice[21]. Here we show that mPFC-LHA
388 pathway activity in relation to food intake depends on the frequency used, with 5Hz stimulation
389 driving increased intake of specifically palatable food. Our study also reveals a food type
390 dependency for the role of mPFC-LHA in feeding. Our feeding assay was a 2-choice paradigm
391 where the ad libitum fed mice could either choose between familiar palatable fat or chow.
392 Notably, 5Hz stimulation of the pathway only altered fat intake but not chow intake. This
393 suggests that the circuit manipulations caused a directed increased drive towards palatable
394 foods, rather than an indiscriminate urge to chew. Finally, our data suggest that internal
395 (satiety) states may contribute to the role of mPFC-LHA pathway in food intake. We observed
396 that the 5Hz manipulations did not cause altered food intake during the early stimulation
397 blocks, when the drive for food intake was relatively high. Instead, it was only in later phases
398 that pathway stimulation resulted in increased time spent eating. A possible interpretation is
399 that mPFC-LHA pathway activity can contribute to continued feeding engagement and/or that it
400 counteracts the experience of satiety. With regards to engagement, recent evidence suggests
401 that cortical inputs to the hypothalamus encode behavioral transitions[41]. With regards to
402 satiety, our experiments were notably all performed in ad libitum-fed animals such that satiety

403 states may have occurred more readily. Interestingly, also in stressed mice, which in normal
404 circumstances exhibited an immediate binge-like profile, optogenetic stimulation of the mPFC-
405 LHA pathway left this extent of bingeing intact (and did not exacerbate it), but strikingly then
406 such stimulation maintained recurrent intake later on, when the drive towards food for
407 unstimulated stressed mice had already abated.
408
409 The chemogenetic data regarding experiments performing mPFC-LHA inhibition are also in
410 accordance with such a conditional role of this pathway in food intake. Inhibition of the
411 pathway under normal conditions did not alter food intake, of neither chow nor fat, in
412 accordance with an earlier study[21]. Instead, we show that after a social stress experience that
413 drives excess intake of specifically palatable food (hyperphagia)[3], inhibition of the pathway
414 abolishes only the amount of excess fat intake due to stress. Aside from the hyperphagic effects
415 occurring hours-days after social stress days[24], there are also short-lived hypophagic effects
416 immediately during the stress (i.e. reduced feeding). Chemogenetic inhibition of the mPFC-LHA
417 pathway did not modulate such acute social stress-driven hypophagia. Notably, a previous study
418 reported that under different mild anxiogenic conditions (e.g. novel foods, or novel feeding
419 environments) mPFC-LHA inhibition could prevent reductions in food intake[21]. This apparent
420 discrepancy on the role of mPFC-LHA in stress-driven hypophagic responses may be due to
421 either the type of stressor (i.e. novelty versus social stress) or due to the intensity of the stress
422 (i.e. mild anxiety from novelty, or stronger fight-or-flight like responses). Overall, we propose
423 that mPFC-LHA activity is not indispensable for regular (palatable) food intake, but is important
424 for heightened palatable food intake upon stress.
425
426 <u>The mPFC-LHA is not a singular pathway: circuit framework for heterogeneous function</u>
427 If mPFC-LHA pathway activity does not have a uniform relation to food intake, then what are the
428 underlying biological underpinnings of this? We propose that the large functional anatomical
429 heterogeneity of mPFC-LHA circuits is at the heart of this. Rather than a singular pathway, we
430 now show that the mPFC-LHA connection is composed of multiple branches, that can have
431 diverse functions. Indeed, we observed that mPFC projections innervate multiple LHA

432 subpopulations based on LHA cell type. We observed strong connectivity with LHA_{VGAT} and
433 LHA_{VGLUT2} neurons. Furthermore, we observed strong connectivity with functionally distinct LHA
434 subpopulations such as LHA_{OREX} and LHA_{MCH} neurons. Our findings show that stimulation or
435 inhibition of mPFC-LHA pathways will affect multiple network branches at the same time. It is
436 interesting to speculate that distinct frequencies of stimulation of mPFC-LHA pathway may
437 strike a different balance between engagement of these multiple subbranches. We observed
438 that food intake was most increased with 5Hz stimulation of mPFC-LHA pathways. Interestingly,
439 a previous study reported that 5Hz optogenetic stimulation of LHA_{VGAT} projections to the VTA
440 could optimally drive food intake, with neither 2.5Hz nor 20Hz causing any changes in food
441 intake[19]. Possibly a 5Hz mPFC-LHA stimulation proportionally favors engagement of branches,
442 such as $mPFC_{GLU}$-LHA_{VGAT}-VTA to promote food intake, whereas for other stimulation
443 frequencies a different mixture of branch engagement is reached with no alterations in food
444 intake or even decreases[21]. In accordance with this idea, we found here that mPFC-innervated
445 LHA_{VGAT} neurons showed, particularly at relatively lower current input, the highest excitability
446 out of the major LHA populations we tested.
447
448 <u>The mPFC-LHA pathway as a (social) stress integrator</u>
449 Recent studies have shown that the mPFC-LHA pathway is sensitive to social information[20,31,42],
450 and bulk population-level recordings showed that the pathway exhibits calcium responses to an
451 air puff[21]. Here we captured single cell dynamics of mPFC cells projecting to the LHA during
452 social stress experiences with *in vivo* electrophysiology. We observed a heterogeneous response
453 of these cells. We also leveraged ensemble-tagging technology to show that stress-reactive
454 mPFC cells directly project to the LHA. We show that the mPFC cells reactive to acute stress (in a
455 timeframe where hypophagia occurs) project less onto LHA_{VGAT} neurons, which have an
456 established role in promoting food intake[14,15,17], and more onto LHA_{VGLUT2} neurons and their
457 subtypes (e.g. LHA_{OREX} and LHA_{MCH}). LHA_{VGLUT2} cells, which have a more context-specific role in
458 food intake, but often suppress it[3,43]. The TRAPed $mPFC_{ACUTE\ STRESS}$-LHA ensemble may not fully
459 correspond one-to-one with the mPFC-LHA cells that, in the *in vivo* electrophysiology
460 experiment, exhibited acute activation during the social stress. Nevertheless, these two findings

461 together suggest that during the hypophagia of an acute social stress, mPFC cells that project to
462 LHA_{VGAT} cells may exhibit reduced or unchanged activity, whereas mPFC cells that project to
463 LHA_{VGLUT2} cells (and its subtypes) are acutely recruited. Interestingly, LHA_{VGLUT2} cellular
464 populations are also those at which we observe social stress-driven synaptic plasticity
465 afterwards (general weakening), when the stress effects turn into hyperphagic responses. It is
466 plausible that the initial response to acute stress partakes in the induction mechanism towards
467 subsequent synaptic plasticity. The involved cascades in this process remain an interesting topic
468 for further studies.
469
470 Stress-driven plasticity within mPFC-LHA circuits
471 After social stress, at a time point where mice would overeat[3], we observed changes indicative
472 of reduced release probability selectively at mPFC synapses onto LHA_{VGLUT2} neurons.
473 Interestingly, many LHA_{VGLUT2} cells are linked to a role in curtailing food intake[15,17].
474 Consequently, a reduction of the excitatory input on such neurons could be in accordance with
475 a weakening of a brake on the drive for food intake. A finer grained analysis revealed that the
476 effect of stress on mPFC synapses onto LHA_{VGLUT2} cells was further dependent on the projection
477 targets of the hypothalamic cells. We observed evidence for weakened $mPFC_{GLU}$ synapses onto
478 those LHA_{VGLUT2} cells projecting to a midline hypothalamic region, which indeed upon
479 stimulation curtails food intake[44]. Oppositely, we found that $mPFC_{GLU}$ synapses onto LHA_{VGLUT2}
480 cells projecting to the VTA exhibit potentiation after stress. This latter finding is in accordance
481 with our recent report that after social stress LHA_{VGLUT2} projections to VTA dopamine neurons
482 become potentiated and that this plays a causal role in excess food intake[3]. LHA_{VGLUT2} cells have
483 several more projection targets than the ones investigated here[45], which may also be changed
484 by stress. Therefore, the analysis of these specific projections is not meant to be exhaustive, but
485 it illustrates that mPFC synaptic contacts onto distinct LHA_{VGLUT2} subpopulation are divergently
486 affected by social stress. It also illustrates that this can occur in a manner where both a
487 subsystem linked to reducing food intake gets weakened, while a subsystem linked to increasing
488 stress-driven food intake get strengthened.
489

490 Overall, our work identifies the mPFC-LHA pathway as a critical node driving overconsumption
491 of fat after stress and emphasizes that mPFC interactions with the LHA are multi-form to
492 provide a flexible system with a conditional, situation-dependent, role in (stress-driven) food
493 intake.
494

495 **Material & Methods**

496

497 **Animals**

498 In all experiments naïve adult male mice were used (20-35 g, >6 weeks). C57Bl6J (Jax #664),
499 Vglut2-Cre[46] heterozygous (Jax #28863), VGAT-Cre[46] heterozygous (Jax #016962) and TRAP2
500 heterozygous[29] (Jax #030323), animals were bred in-house but originated from the Jackson
501 Laboratory. Swiss-CD1 mice (35-45 g, >12 weeks), were purchased from Janvier (France). All
502 mice (except Swiss-CD1 mice) were group-housed (2-5 per cage) unless otherwise specified.
503 Mice were housed in a 12:12 light/dark cycle (lights on at 07:00 a.m.) at 22 ± 2° C (60-65%
504 humidity). Unless otherwise specified (during brief binge eating recording sessions, see below),
505 animals had access to ad libitum water and lab chow (3.61 kcal/g, CRM (E), 801730, Special
506 Diets Services). Experiments were approved by the Animal Ethics Committee of Utrecht
507 University, and by the national authority (CCD). Experiments were conducted in agreement with
508 the Dutch law (Wet op de Dierproeven, 2014) and the European regulations (Guideline
509 86/609/EEC).

510

511 **Stereotaxic surgery**

512 For stereotactic surgery, all mice were anesthetized with ketamine (75mg/kg i.p.; Narketan,
513 Vetoquinol) and dexmedetomidine (1mg/kg i.p.; dexdomitor, Vetoquinol). Lidocaine (0.1ml;
514 10% in saline; B. Braun) was injected under the skin on the skull a few minutes before surgery.
515 Eye ointment cream (CAF, Ceva Sante Animale B.V.) was applied before surgery. All mice were
516 at least 6 weeks of age at the time of surgery. Animals were fixed on a stereotactic frame (UNO
517 B.V.) and kept on a heat pad during surgery (33° C). When animals were implanted with either
518 optic fibers or cannulas the skull surface was scratched with a scalpel and phosphoric acid (167-
519 CE, ultra-Etch, ultradent, USA) was applied for 5 minutes to roughen the surface at the start of
520 surgery. Injections were done using a 31G metal needle (Coopers Needleworks) attached to a 10
521 µl Hamilton syringe (model 801RN) via flexible tubing (PE10, 0.28 mm ID, 0.61 mm OD, Portex).
522 The Hamilton syringe was controlled by an automated pump (UNO B.V. -model 220). Injections
523 were done bilaterally unless otherwise specified and volumes ranged between 250 and 300 nl

524 per side, at an injection rate of 100 nl/min. The injection needle was retracted 100 µm, 9 min
525 after the infusion and withdrawn completely 10 min after the infusion. The skin was sutured
526 post-surgery (V926H, 6/0, VICRYL, Ethicon). Animals were then subcutaneously injected with the
527 dexmedetomidine antagonist atipamezole (50 mg/kg; Atipam, Dechra), carprofen (5 mg/kg,
528 Carporal) and 1 ml of saline and left to recover on a heat plate of 36° C. Carprofen (0.025 mg/L)
529 was provided in the drinking water for one week post-surgery. Animals were single-housed
530 post-surgery and rejoined with their cage mates three days after surgery, unless otherwise
531 stated.
532
533 *For ex vivo optogenetic-assisted electrophysiology experiments:*
534 For transgenic lines: VGAT-Cre and Vglut2-Cre, mice were injected with AAV5-Syn-CoChR-GFP
535 (3.8*10^12 gc/ml; 300nl; UNC Vector Core) in mPFC (+1.8mm anterior to bregma; 0.90 mm
536 lateral; -2.2 mm ventral from skull under an angle of 10°) and injected with AAV5-hSyn-DIO-
537 mCherry (3*10^12 gc/ml; 300nl; Addgene) in LHA (-1.3 mm posterior to bregma; 1.9 mm lateral;
538 -5.4 mm ventral from skull under an angle of 10°) to visualize GABAergic neurons in VGAT-cre
539 mice and glutamatergic neurons in Vglut2-cre mice.
540 To visualize neuropeptide populations in LHA, we used C57bl6 mice, they were injected with the
541 same protocol for the mPFC than the Vglut2-cre and Vgat-cre. Mice were injected with rAAV5-
542 MCHpr-Gq-mCherry (1*10^12 gc/ml) for labelling the MCH populations and with AVV5-
543 hORXpr1-3TdTomato (1*10^12 gc/ml) for the Orexinergic neurons. Both were injected in the
544 LHA with the same coordinate and volume than for the transgenic mice.
545 To identified glutamatergic LHA neurons projecting to LHb, VTA and ADMH, we used a cre-
546 dependent retrograde tracer retroAAV-hSyn-DIO-mCherry (2.8*10^12 gc/ml; Addgene) in
547 Vglut2-cre mice. Mice were then injected in one of these areas: in the LHb (-1.6 mm posterior to
548 bregma; 1.2 mm lateral; -3.05 mm ventral from skull under an angle of 15°), in VTA (-3.2 mm
549 posterior to bregma; 1.65 mm lateral; -5.0 mm ventral from skull under an angle of 15°) and
550 ADMH (-0.8 mm posterior to bregma; 1.1 mm lateral; -5.4 mm ventral from skull under an angle
551 of 10°). Mice were also injected in mPFC with AAV5-Syn-CoChR-GFP.
552

553

554

555 *For ex vivo TRAP-assisted electrophysiology experiments:*

556 VGAT-cre::TRAP2 and Vglut2-cre::TRAP2 mice were first injected in mPFC with rAAV5-Syn-Flex-
557 CoChR-GFP (4.4*10^12 gc/ml; UNC Vector Core). After a minimum of two weeks, mice went
558 under stress and tamoxifen i.p injection (25mg/kg). After a minimum of one week, mice were
559 injected in LHA with AAV5-hSyn-DIO-eGFP (1*10^12vc/ml; Addgene) and co-injected with
560 rAAV5-ORXpr1-3TdTomato (1*10^12 gc/ml) or rAAV5-MCHpr-Gq-IRES-mCherry (1*10^12
561 gc/ml).

562

563 *For in vivo optogenetic experiments:*

564 To drive the mPFC-LHA pathway at various frequencies, C57BL6 mice > 3 months of age were
565 bilaterally injected with the light-sensitive Channelrhodopsin variant CoChR (300 nl rAAV5-Syn-
566 CoChR-GFP at a titer of 3.8*10^12 gc/ml) or a fluorophore for control animals (300 nl rAAV5-
567 Syn-eYFP, titer of 5.6*10^12 gc/ml) (Penn Vector Core, USA) in the mPFC (AP +1.8; ML ±0.92
568 mm from bregma; DV -2.24 mm from the skull at a 10° angle; 100 nl/min). After injection a 10-
569 min delay was implemented and, two minutes before retraction, the needles were lifted 100
570 micrometers to allow for proper diffusion of the virus. To stimulate mPFC axon terminals
571 innervating the LH, optic fibers (diameter 200 µm; FT200UMT, 0.39NA, Thorlabs, Germany)
572 fitted with ceramic ferrules (230µm bore size, Precision Fiber Products, MM-FER2002, USA or
573 Thorlabs, CFLC230-10, Germany) were targeted to the lateral hypothalamus and implanted
574 bilaterally at AP -1.2; ML ±1.85 from bregma and DV -4.85 mm from the skull under a 10° angle.
575 The implants were fixed to the skull using 2 stainless steel screws, C&B-Metabond (Parkell Inc.,
576 USA), and dental cement (GC Corporation, Japan). After surgery mice were individually housed
577 for the remainder of the experiment.

578

579 *For in vivo chemogenetic experiments*

580 The pAAV-hSyn-DIO-hM4D(Gi)-mCherry (DREADD virus) (4*10^12 gc/ml, Addgene, United
581 States, addgene.org) or pAAV-hSyn-DIO-mCherry (4.2*10^12 gc/ml, Addgene, United States,

582 addgene.org) were bilaterally injected into the mPFC, (in mm: +1.8AP, -1.2ML from Bregma and,
583 -2.3 DV, from skull, at a 10° angle) with an injection-rate of 100 nl/min, and a volume of 300 nl.
584 The Cav2-cre-virus (2*10^12 gc/ml, Plateforme de Vectorologie de Montpellier, https://plateau-
585 igmm.pvm.cnrs.fr/), combined with red-retrobeads (60x dilution, Lumafluor Inc, lumafluor.com)
586 for injection site verification, was bilaterally injected into the anterior LHA (in mm: -1AP,
587 1.85ML, 5.36DV from Bregma, at a 10° angle), and posterior LHA (in mm: -1.85AP, 1.9ML,
588 5.41DV, from Bregma, at a 10° angle) with an injection-rate of 100nl/min. After injection of the
589 viral construct, the needle was kept in place for 8 minutes after which it was retracted for 100
590 um and left in place for two more minutes to allow proper diffusion of the virus. Thereafter, the
591 needle was fully subtracted at a slow pace. After injection, the skin was sutured (V926H, 6/0,
592 VICRYL, Ethicon). After surgery mice were individually housed for the remainder of the
593 experiment.
594
595 *For in vivo electrophysiology with optrode experiments*
596 To identify mPFC neurons that project to the LHA in electrophysiological recordings we used a
597 dual viral approach. First the Cav2-cre-virus (2*10^12 gc/ml, Plateforme de Vectorologie de
598 Montpellier, https://plateau-igmm.pvm.cnrs.fr/) was injected, combined with red-retrobeads
599 (60x dilution, Lumafluor Inc, lumafluor.com) for injection site verification, into LHA (in mm: -
600 1.3AP, 0.9 ML, -5.3DV from Bregma, 0° angle). A second virus pAAV-EF1α-doublefloxed-
601 hCHR2(H134R)-mCherry was injected at two locations in the mPFC (+1.8 mm AP, -0.45 mm ML, -
602 2.5 mm DV and +1.8 mm AP, -0.45 mm ML, +1.8 mm AP from Bregma, 0° angle, 100-150nl per
603 site and a titer of 2-4*10^12 gc/ml). All injections were done unilateral and targeting the left
604 hemisphere, except for 2 mice which received a bilateral injection in the LHA. Injections for
605 electrophysiological recordings were done using glass pipettes (#504949 , World precision
606 instruments) coupled to a Nanojet injector (#504127, World Precision Instruments). To allow for
607 proper expression of the virus before electrophysiological recordings, the optrode was placed in
608 a second surgery, >3 weeks after viral injections, in the left mPFC (+1.8mm AP, -0.5mm ML from
609 Bregma, -2.0mm DV from the surface of the brain). During this surgery a craniotomy was made
610 above the mPFC and the dura removed, whereafter the optrode was inserted in the brain using

611 a micromanipulator (Scientifica, UK). Two screws were placed in the skull for attachment of the
612 optrode to the skull and the ground was placed through a small hole in the skull on the
613 cerebellum and fixed with a small drop of superglue. After closure of the craniotomy with
614 silicone, the whole implant was fixed with C&B-Metabond (Parkell Inc., USA), and dental cement
615 (GC Corporation, Japan). Recordings during behavior were made at least 3 weeks after
616 implantation of the optrode to allow for proper recovery. After surgery mice were individually
617 housed for the remainder of the experiment.
618
619 **Patch-clamp Electrophysiology**
620 Mice were anesthetized with isoflurane (Zoetis, UK) in the morning and were then rapidly
621 decapitated. Coronal brain slices of 250 µm were cut on a vibratome (1200 VTs, Leica, Rijswijk,
622 The Netherlands) in ice-cold carbogenated (95% O2, 5% CO2) cutting solution, which contained
623 (in mM) choline chloride (92); ascorbic acid (10); CaCl2 (0.5); glucose (25); HEPES (20); KCl (2.5);
624 N-Acetyl L Cysteine (3.1); NaHCO3 (25); NaH2PO4 (1.2); NMDG (29); MgCl2 (7); sodium pyruvate
625 (3); Thiourea (2). Slices were transferred for 5-10 min to a warmed solution (34 °C) of the same
626 composition, before they were kept at room temperature in carbogenated incubation medium,
627 which contained (in mM): ascorbic acid (3); CaCl2 (2); glucose (25); HEPES (20); KCl (2.5); NaCl
628 (92); NaHCO3 (20); NaH2PO4 (1.2); NMDG (29); MgCl2 (2); sodium pyruvate (3) and Thiourea
629 (2). During recordings, slices were immersed in artificial cerebrospinal fluid (ACSF) containing (in
630 mM): NaCl (124); KCl (2.5), CaCl2 (2.5); glucose (11); HEPES (5); NaHCO3 (26); NaH2PO4 (1);
631 MgCl2 (1.3) and were continuously superfused at a flow rate of 2 ml min−1 at 32° C.
632
633 Neurons were patch-clamped using borosilicate glass pipettes (2.7–4 MΩ; glass capillaries,
634 GC150-10, Harvard apparatus, UK), under a BX51WI Olympus microscope (Olympus, France).
635 For voltage or current clamp recordings, signal was amplified, low-pass filtered at 2.9 kHz with a
636 4-pole Bessel filter and digitized at 20 kHz with an EPC9/2 dual patch-clamp amplifier (HEKA
637 Elektronik GmbH). Data were acquired using PatchMaster v2x78.2 software. After break-in, 10
638 minute waiting time occurred prior to the start of the recording. Series resistance was
639 determined in Voltage clamp with a −4 mV step from -65 mV to -69 mV lasting 50 ms, using the

640 resultant capacitive current transients and Ohm's law. Light pulses (470 nm, 1 ms; 25.4mW)
641 were delivered with a pE-4000, CoolLed, UK illumination system. All electrophysiological
642 measures are recorded with a 10 seconds inter sweep interval (0.1Hz) and all data points are
643 shown as an average of 10-20 sweeps, unless otherwise specified.
644
645 *Paired-pulse ratio (PPR):* PPR experiments were performed with cesium methanesulfonate-
646 based internal medium, containing (in mM) cesium methanesulfonate (139), CsCl (5), HEPES
647 (10), EGTA (0.2), creatine phosphate (10); Na2ATP (4); Na3GTP (0.3); MgCl (2 2). Averaged
648 AMPAR-mediated currents in LHA neurons were measured in response to optogenetic
649 stimulation of mPFC terminals using two pulses with a 60, 100 or 200 ms inter-pulse interval and
650 measuring the resulting peak amplitude of the two synaptic responses. The PPR was calculated
651 by dividing the amplitude of the synaptic response to the 2nd pulse by the amplitude of the
652 synaptic response to the 1st pulse.
653
654 *NMDAR-AMPAR ratios:* Synaptic LHA optogenetically evoked AMPAR and NMDAR currents were
655 measured in response to a single light pulse. Recordings were made in voltage clamp with the
656 aforementioned cesium methanesulfonate-based internal medium. Under these conditions, it
657 was possible to detect inward glutamatergic currents (at −65 mV) and NMDAR (at 40mV at 100
658 ms). Experiments were done in the presence of 100 µM picrotoxin, to block potential $GABA_A$
659 receptor contributions. The NMDA/AMPA ratio was calculating by dividing the amplitude of the
660 EPSC after 100ms at +40mV by the amplitude of the synaptic response at -65mV.
661
662 *mPFC-LHA connectivity experiments*: Recordings were made in voltage clamp in a cesium
663 methane sulfonate based internal medium as described above. Under these conditions, it was
664 possible to detect inward glutamatergic currents (at −65 mV). Cell type specific connectivity was
665 determined based on whether a neuron showed an optogenetically-evoked synaptic response
666 larger than 5 pA. For monosynaptic confirmation, cells were recorded and opto-stimulated
667 (1ms) once per sweeps, first during at least 15 sweeps with ACSF, then 1µM of TTX was added

668 to ACSF for a minimum of 25 sweeps to observe the effect on the synaptic response and finally
669 100µM 4-AP was added to the mix and recorded for a least 20 sweeps.
670
671 *Intrinsic excitability and mPFC-driven LHA cell firing experiments:* Recordings were made in
672 current clamp in a potassium gluconate based internal containing (in mM), Potassium Gluconate
673 (139); HEPES (10); EGTA (0.2); creatine phosphate (10); KCl (5); Na2ATP (4); Na3GTP (0.3); MgCl2
674 (2). Only LHA cells showing a synaptic response larger than 5pA at -65mV after 1ms of opto-
675 stimulation went under this following protocol. To determine current-voltage relationships and
676 biophysical properties, membrane resistance and firing pattern, cells were recorded in current
677 clamp. Cells were clamped at 0 pA and from there were subjected to 17 subsequent sweeps.
678 Every sweep started with a 0 pA injection of 400 ms, followed by a current step of 800 ms length
679 of -150 pA (with a +25 pA increasing increment on each subsequent sweep), followed by a
680 return to 0 pA for 1000 ms. Inter-sweep interval was 10 seconds.
681 To assess if the opto-stimulation of mPFC inputs was sufficient to fire the LHA neurons, cells
682 were clamped at -50pA to prevent the spontaneous firing and 25 pulses of 1ms were applied at
683 5Hz for 10 sweeps.
684
685 *Drugs for patch-clamp experiments*
686 All drugs were obtained from Sigma (UK), Abcam (UK) and Tocris (UK). With the exception of
687 picrotoxin (DMSO, 0.01% final bath concentration) all drugs were dissolved in purified water.
688 Drugs were aliquoted at a concentration of 1/1000th of the final bath concentration and stored
689 at -20°C. Upon use they were thawed and quickly dissolved in the recording medium.
690
691
692 ***In vivo* electrophysiology recordings**
693
694 *Recording single unit activity of prefrontal cortical neurons.*
695 Extracellular single-unit activity was recorded using custom-build optrodes. An electrode bundle
696 consisting of 32 individually isolated nichrome wires (12 µm diameter; 80% nickel, 20%

697 chromium; Kanthal, Sandvik Material Technology, Germany) was glued to an optic fiber
698 (Thorlabs, Germany, 200 µm diameter, 0.39NA, with the tip placed at 300-700 µm above the
699 electrodes) to allow for optogenetic identification of mPFC-LHA cells. Electrodes were attached
700 with gold pins to a 32-pin Omnetics connector using an electrode interface board (Open Ephys,
701 www.openephys.org) which was mounted on a 3D printed holder (based on the Flexdrive[47],
702 Open Ephys). The microwires were cut at an angle so that they were organized in a vertical
703 space of 200-400 µm, whereafter they were gold-plated (Neuralynx, United States) to an
704 impedance of 100kΩ using a NanoZ impedance tester (Plexon, United States). The connector
705 was grounded through a bare platinum-iridium wire (127 µm diameter; 90% platinum, 10%
706 iridium; Science Products, Germany) placed on the cerebellum. Analog signals were acquired
707 using a 32-channel RHD2132 headstage (Intan Technologies, USA), bandpass filtered between
708 2.5 and 7603.88Hz, and digitized at 30 kHz. Data were transferred to the Open Ephys acquisition
709 board using an Intan Technologies Serial Peripheral Interface cable (2.9 mm, interference of the
710 cable during behavior was reduced by counterbalancing the weight of the cable with flexibly
711 moving counterweights) and acquired by the Open Ephys GUI interface (version 0.5.2.2;
712 https://open-ephys.org/gui)[48]. Behavior of the mice was recorded from above the cage using a
713 Blackfly S USB camera (BFS-U3-31S4M-C, Teledyne FLIR) which was synchronized with the
714 electrophysiological data by sending a TTL pulse for every acquired frame (sample rate 30Hz) to
715 the Open Ehpys I/O board. The mice were also recorded front view using a webcam (HD C270,
716 Logitech, Switzerland). This data was synchronised by a light signal generated at a fixed interval
717 by an Arduino controlled LED which light signal was duplicated as a TTL output to the I/O board.
718
719 *Spike sorting.*
720 Before spike-sorting first a common average reference (https://github.com/cortex-
721 lab/spikes/blob/master/preprocessing/applyCARtoDat.m) [49] was applied to remove common
722 noise contamination across channels. Spikes were then automatically detected and assigned to
723 clusters using the template-matching algorithm of kilosort (version 2.0;
724 https://github.com/MouseLand/Kilosort/releases/tag/v2.0) with the following settings: Ops.Th
725 [10 4], Ops.AUCsplit [0.9], ops.Lam [10], ops.minFR [0.1]. Clustering results were manually

726 checked for waveform shape, stable amplitude over time and the presence of a clear refractory
727 period. Moreover, resembling clusters were assessed to see if nearby clusters belonged to the
728 same cell and were merged when appropriate. Data checking and curation was done in Phy
729 (https://github.com/cortex-lab/phy). After curations in Phy the isolation distance was calculated
730 as a final quality control. Single units with an isolation distance of >20 were included in the
731 dataset [50,51] (Average isolation distance of optotagged mPFC-LHA cells=38.5, Minimum=20.9,
732 Maximum=115.2).
733
734 *Optogenetic identification of mPFC-LHA neurons.*
735 After every behavioral session, we applied short light pulses (2ms) from a 473 nm DPSS laser
736 (CNI Laser, China) with a random 6-9 s interval for ~30 min (over 200 trials) triggered using a
737 microcontroller (Arduino, Italy)) and ~5-8 mW output at the fiber tip above the recording site.
738 Depending on the presence of a voltage-volley during laser stimulation, a window of 1 or 2 ms
739 after the laser onset was blanked. Significant light-induced activation was determined with the
740 stimulus-associated spike latency test (SALT, $P < 0.01$; http://kepecslab.cshl.edu/salt.m)[50]. In
741 brief, SALT compares the distribution of first spike latencies relative to the light pulse to epochs
742 of the same duration in the stimulus-free baseline period. Additional criteria were included to
743 prevent inclusion of false-positive neurons through network-related activity: a peak z-
744 score>1.65, average first spike latency < 7ms, jitter < 3.5ms, reliability > 0.03, Pearson's
745 correlation between the average waveform of a cluster and the average waveform of the first,
746 putatively light-evoked spikes > 0.8 and a waveform duration above 550 microseconds. Similar
747 criteria have been used for mPFC-LHA opto-tagging and ex-vivo data of mPFC-LHA neurons
748 suggest that a first spike latency below 8ms limits false-positive identification of non-expressing
749 neurons through recurrent connectivity [20] and the same criteria were also used in other mPFC
750 opto-tagging studies[50,52,53]. According to these criteria mPFC-LHA neurons could be photo-
751 identified in 6 out of 10 mice that had correct placement of the optrode and proper expression
752 of channelrhodopsin.
753
754 **Behavioral paradigms**

755 All behavioral manipulations and tests were performed during the light phase.

756

757 *Two-day Social stress paradigm*

758 The social subordination stress protocol used was designed according to a resident intruder
759 paradigm. The resident, a Swiss-CD1 male previously used for breeding, was housed in a large
760 Makrolon cage (type IV, Tecniplast, Italy), an intruder; an experimental male mouse, was placed
761 in this cage. Fighting time was tracked live and animals were allowed to fight for 20 s, twice a
762 day for two days, one fighting session in the morning (8.30 – 11.00a.m.) and one in the
763 afternoon (16.00 – 18.30p.m.). For the remainder of the day, animals were separated by a
764 perforated transparent splitter, allowing sensory, but no physical interaction. The control
765 animals were co-housed with a non-familiar C57B6J male mouse for two days, preventing
766 physical interaction. This short stress paradigm has been shown to not change body weight in
767 the first days after the stressful experience when food intake is measured[3]. Consistent with this,
768 no difference in body weight were observed between the experimental groups in this study.

769

770 *Limited access choice diet*

771 In the limited access choice diet paradigm, animals were exposed to fat (i.e. tallow; Blanc de
772 Boeuf, Vandermoortele, 9.0 kcal/g) and regular chow for 2 hours a day in a clean cage
773 (Makrolon cage type IV, Tecniplast, Italy). Animals were habituated to the limited access cage
774 and fat, during 3 occasions at least, before the start of the experiment. Animals were subjected
775 to stress as described above and on the day after, fat intake was measured over a 2-hour fat
776 access period, starting between 9 a.m. and 11 a.m.. Unlimited chow was provided the remaining
777 22 h of the day.

778

779 *Real-time place preference / aversion test*

780 The conditioned place preference test consisted of two sessions separated over two days. The
781 test cage (73x25 cm) consisted of two chambers (30x25 cm) clearly separated by a narrower
782 middle area. The two chambers had different flooring (fine grid vs coarse grid) and different
783 walls (striped vs black) to provide contextual discriminability. In the baseline session mice were

allowed to freely explore the test cage. During the test session (20 minutes total duration) one of the compartments (counterbalanced design) was paired with optogenetic stimulation using closed-loop optogenetics. After 10 minutes the stimulation site was paired with the other compartment, to limit effects of a priori preference for one of the compartments. Mice were recorded by a webcam (HD C270, Logitech, Switzerland). Closed-loop optogenetics was established by automatically tracking mice in Bonsai (Open Ephys) which triggered the Master-8 pulse generator through an Arduino upon entering the stimulation chamber, in turn triggering the laser at the dedicated frequency as long as the mouse was present in the stimulation compartment. The position of the animal was tracked in the cage offline using Ethovision 9 (Noldus, Wageningen). Preference score was calculated by scoring the total time spent in the stimulation compartment divided by the total time spent in the stimulation and non-stimulated compartment. Cages were cleaned in between animals with 70% ethanol.

Food intake video analysis

Videos were taken from the side of the feeding cage with webcams (HD C270, Logitech, Switzerland) and acquired using the Windows Camera App or Bonsai. Feeding bout analysis was done manually and blind for the virus type. Data were acquired over different batches which were analyzed by an independent observer.

Recordings during social stress.

For social stress recordings mice were handled extensively to get used to fixation and getting used to being attached to the recording cable. During the day of social stress recordings mice were put into an unfamiliar cage of a CD1 aggressor mouse, which was temporarily removed from its home cage. After 15 minutes the CD1 mouse was introduced into the cage but physical contact was prohibited by a transparent barrier. After another 45 minutes the barrier was re moved and the mice were allowed to physically interact (fight) for a cumulative 20 seconds whereafter the barrier was put back. This period lasted on average more than 4 minutes. Hence, during the total stress exposure time physical contact which could introduce noise in the recording was limited.

813

814 *Locomotor activity and time spent in food zones.*

815 Mice position and speed in the food cage were automatically tracked in real-time from camera
816 images or offline from the acquired webcam videos using Ethovision (version 9.1; Noldus
817 Technologies, The Netherlands). Food zones were 9x11 cm in size. Time in the food zone was
818 determined by calculating the cumulative time spent in the food zone per 10 minute block. The
819 effect of 5Hz stimulation on time in food zone was determined by calculating the difference in
820 time spent in the food zone during the individual three ON-Blocks with the preceding OFF-block
821 and consequently taking the average of these three values obtained for the separate ON-Blocks.

822

823 ***In vivo* circuit manipulation and food intake experiments**

824

825 *In vivo optogenetic stimulation experiment in stress-naïve mice*

826 Before every experiment, mice were extensively handled and habituated to the food-context,
827 fat and optogenetic cables for at least 2 weeks before the start of the experiment. A single
828 experiment consisted of three baseline days, an optogenetic stimulation day followed by
829 another non-stimulation day. Mice were also attached to patch cables on days where no
830 stimulation was applied. Raw food intake was measured on all days after one hour in which the
831 mice were able to freely feed on regular chow (3.61 kcal/g, CRM (E), 801730, Special Diets
832 Services) or Tallow (Blanc de Boeuf, Vandemoortele, 9,0 kcal/g). On stimulation days mice were
833 recorded with a webcam from the top, to allow for later offline tracking of the position of the
834 mice in the food cages using Ethovision (Noldus, Netherlands). In a subset of the experiments
835 feeding behavior was recorded from the side using webcams (HD C270, Logitech, Switzerland).
836 Time of testing across days was kept constant as much as possible. Different frequencies were
837 tested on the same mice and in the order 5Hz, 10Hz and 1Hz with one week without stimulation
838 in between each stimulation experiment.

839

840 On stimulation days, mice were connected to optogenetic patch cables (Thorlabs, 200 µm, 0.39
841 NA, FT200UMT) which ended in a ceramic ferrule (230 µm bore size, Thorlabs or Precision Fiber

842 Products) and connected to the implant through a sleeve (Precision Fiber Products). Cables
843 were connected to the laser (473 nm DPSS laser, CNI Laser, China) using an FC-connector
844 (Thorlabs) and via a rotary joint (Doric lenses, Canada), which divided light intensity equally over
845 the two hemispheres. Light intensity was set to 5mW at the tip of the fiber above the LHA. Light
846 pulses (5ms duration) at indicated frequencies were applied during blocks of ten minutes using
847 a Master-8 pulse stimulator (A.M.P.I., Jerusalem, Israel) and were alternated with non-
848 stimulation blocks of similar length. Mice were single-housed and food and water were present
849 ad libitum in the home cage.
850
851 *In vivo optogenetic stimulation experiment control versus stressed mice*
852 Experimental setup for optogenetic stimulation is similar as described above. 5Hz stimulation
853 was applied in alternating OFF and ON blocks with a duration of ten minutes. Mock-stimulated
854 animals were attached to patch-cables and laser-stimulated, but light transmission was
855 completely blocked in the connecting sleeve on the head of the animal. For this experiment in
856 particular, mice were habituated to fat (three times) in the food context and to optogenetic
857 cables in the test cage for two weeks. Baseline food intake was measured 4-5 days before
858 exposure to stress. During this session animals were similarly attached to patch cables but no
859 stimulation was applied. Social stress paradigm was performed as described[3]. C57BL6 mice were
860 introduced into a cage (Makrolon cage, type IV, Tecniplast, Italy) of an aggressor mouse (CD1,
861 Janvier) and subjected to 4x 20s of physical fight over the course of two days (one fight in the
862 morning and one in the afternoon) after which they were separated by a transparent wall for
863 the remainder of the time. The cage of the Swiss-CD1 male mice contained enrichment that was
864 previously used in the home cage, while the cage part of the experimental C57BL6 mice was
865 enriched with 3 tissues. Food and water were present ad libitum as in the stress and home cage.
866 Control mice were subjected to 2 days of cohousing with a conspecific in the same cage, but
867 separated by a transparent wall. On the day after stress mice were put directly from the stress-
868 context into the food context and returned to their home cage afterwards. One mouse was
869 excluded from analysis on the basis of being a large statistical outlier. Three mice were excluded

870 due to technical problems (e.g. malfunctioning video recording). All mice were individually
871 housed during the experiment and had ad libitum access to food and water.
872
873 *In vivo chemogenetic inhibition experiment control versus stressed mice*
874 Mice were extensively handled and habituated to the food context (3 times) and fixation and
875 mock intraperitoneal injections for at least two weeks. First, mice were tested for their baseline
876 fat and chow intake in the 2-choice context (2 hours). For this baseline test, they received an
877 intraperitoneal saline injection (150 µl) to rule-out a potential effect of stress of this procedure.
878 Baseline measurements were done at least 4 days before being subjected to stress to prevent
879 any influence of palatable food intake on their susceptibility to stress. The 2day social stress
880 paradigm was done as described above. CNO was made fresh on the day of testing and applied
881 at a dose of 5 mg/kg, 45 minutes before being placed in the food context. Mice removed from
882 the stress context were injected with CNO and placed back in their home cage with ad libitum
883 food before being put in the food context. Similarly, for the acute stress experiment mice
884 received the CNO injection 45 minutes before being place in the food context and 25 minutes
885 prior to stress. All mice were individually housed during the experiment and had ad libitum
886 access to food and water. Two mice were excluded due to technical problems.
887
888 **Histology and microscopy**
889 For each recording the virus injection sites, as well as the placement of optic fibers and/or the
890 optrodes were examined. Only data obtained from mice with correct placements were included.
891 After experiments, mice were anesthetized with pentobarbital (75-100 mg/kg) and
892 transcardially perfused with Phosphate-Buffered Saline (PBS) containing 4% paraformaldehyde
893 (PFA). Brains were post-fixed in 4% PFA overnight and transferred to PBS. Before slicing, brains
894 were embedded in 4% agarose to maintain structural integrity. Coronal sections of the entire
895 brain were sliced at 60um using a vibratome (VT1000s, Leica, Rijswijk, The Netherlands). For
896 patch clamp experiments out of 272 mice, 27 were excluded on the basis of misinjection of
897 viruses. For behavioral experiments, a total of 6 mice were excluded based on histological
898 assessment.

899

900 *Immunohistochemical staining for histology experiments*

901 To stain for Channelrhodopsin, hM4DGi or control mCherry virus, tissue sections were washed
902 in PBS (0.01 M, pH=7.4) three times for 10 minutes before incubating them for 2 hours with
903 blocking solution (3% BSA, 0.5% Triton-X in 1x PBS). The primary antibody Rabbit Anti-RFP
904 (Rockland, 1:1000 in blocking solution, Lot:46510) that targets mCherry, was administered to
905 the tissue sections using ~400 ul per well. Incubation was carried out overnight at 4 degrees on
906 a shaker to facilitate optimal antibody priming. The next day tissue sections were washed three
907 times with PBS before applying a secondary antibody (goat-anti-Rabbit Alexa-488, Abcam,
908 1:500, Lot:GR3375958-2, Lot:GR3442006-1). The sections were incubated with the secondary
909 antibody for two hours before being washed in PBS again for 3 times. Finally, tissue slices were
910 mounted on glass slides and embedded in FluorSave (Millipore, 345789, Amsterdam,
911 Netherlands) and covered with cover glasses. The microscopy slides were allowed to air dry
912 overnight at room temperature before being stored in a 4-degree environment to maintain
913 sample integrity. For staining of CoChR-GFP anti-GFP antibody was used (Aves, GFP-1020,
914 1:1000 in blocking solution) and goat-anti-chicken Alexa-568 (Abcam, 1:500) as a secondary
915 antibody.

916

917 *Validation of AAV approach to label LHA_{MCH} and LHA_{OREX} cells for patch clamp*

918 Fluorescent cells were co-filled during electrophysiology recording with internal solution and
919 biocytin (2mg/ml). After recording, slices stayed overnight with 4% PFA at 4° C and were then
920 transferred to PBS 0.01% NaAz. For immunolabeling, slices were first wash from NaAz with PBS
921 solution three time for 10min in phosphate-buffered saline (PBS) then blocked 1 hour in room
922 temperature (RT) with blocking solution (10% normal goat serum (NGS) and 5% Triton X-100 in
923 PBS). Followed by overnight at 4°C incubation in primary antibody solution (with 1° antibodies,
924 2% NGS and 0.4% Triton X-100 in PBS). Next day, slices were washed three time during 15 min in
925 PBS, and incubated for three hours at RT with the 2° antibody solution (with 2° antibodies, 2%
926 NGS and 0.4% Triton X-100 in PBS). After, slices were washed three times for 10 minutes in PBS.
927 For the Orexin cells, first antibody used was Rabbit anti-Orexin A (1:1000, Abcam), followed by

928 the secondary antibodies Goat anti-Rabbit 405 (1:500, Abcam) and streptavidin-AF488 (1:500).
929 For MCH cells, slices were stained with Rabbit anti-MCH (1:1000, Sigma-Aldrich, St. Louis, MO,
930 USA) followed by Goat anti-Rabbit 488 (1:500, Abcam) and streptavidin-AF555 (1:500). Cells
931 were imaged with confocal microscope.
932
933 *Microscopy*
934 Slices were imaged using an EPI fluorescence microscope (Axio imager M2, Zeiss) or a confocal
935 microscope (LSM880, Zeiss).
936
937 **Data analysis and statistics**
938 Experimental data were analyzed with (Ethovision V9.0 (Noldus, Netherlands)), GraphPad
939 (version 9.0), SPSS (IBM V26), Python, Igor Pro-8 (Wavemetrics, USA), and Matlab (Mathworks,
940 USA). Experimental sample sizes were predetermined, guided by published studies, in-house
941 expertise, and experimental pilots. Mice were randomly assigned to experimental groups. Mice
942 or data points were not excluded from analyses unless noted. Data graphs are always reported
943 and represented as mean ± SEM, with single data points plotted (single cell for
944 electrophysiology and single animal for behavioral experiments). When statistically appropriate,
945 One-way ANOVAs, Two-way ANOVAs or Multi-way Repeated-measures ANOVAs were applied.
946 Post hoc analyses were performed in case of significant omnibus ANOVA outcomes. In the event
947 the data were not normally distributed statistical testing of group differences was performed
948 using the Kolmogorov-Smirnov test. Testing was always performed two-tailed with α=0.05.
949 Complete outcome of statistical analysis is shown in Supplementary Table 1.
950
951 **Acknowledgements**
952 We thank Fabien Ducrocq, Salvatore Lecca, Manuel Mameli, and the entire Meye Lab for
953 discussions and critical reading of the manuscript. We thank Zoe Bor and Luc Sangers for
954 assistance in analysis and Nicky van Kronenburg for assistance in mouse breedings. This work
955 was supported by (to FM) the ERC under the European Union's Horizon 2020 research and
956 innovation programme (grant agreement 804089; ReCoDE), the NWO VIDI grant 203.102, and

partially by the NWO Gravitation project BRAINSCAPES: A Roadmap from Neurogenetics to Neurobiology (024.004.012) and a Marie-Curie Individual Fellowship (CoMPOSE, grant agreement 898036) to RP.

Author contributions

LS performed and analysed all *ex vivo* electrophysiological recordings. RP performed and analysed behavioral experiments, supported by AB, AN and RH. RP performed and analysed *in vivo* electrophysiological recordings. LS, RP, IWD and ML performed stereotactic surgeries. FM designed the study with RP and LS. FM wrote the manuscript with LS, RP and the help of all other authors.

Corresponding authors

Primary correspondence to Frank J. Meye: f.j.meye-2@umcutrecht.nl

Rogier Poorthuis: rogier.poorthuis@gmail.com

Competing interests statement

The authors declare no competing interests.

Data availability statement

All detailed outcomes of statistical test are provided in Supplementary Table 1. The datasets generated during and/or analysed during the current study are available from the corresponding author on request.

Code availability statement

The codes used for the analyses in the current study have been referenced in the manuscript.

982

983

984 **Figures and Figure legends**

985

986

987

988 **Figure 1. Frequency dependent modulation of palatable food intake by mPFC-LHA pathway**
989 **stimulation. (A)** Experimental timeline and viral and optogenetic strategy to manipulate mPFC-
990 LHA pathway activity. **(B)** Left: Histological verification of CoChR-GFP expression in mPFC and
991 optic fiber location in LHA. Right: mPFC axons in LHA. **(C)** Schematic of behavioral paradigm.
992 Food intake on the test day was measured against three baseline days. On stimulation day
993 mPFC-LHA pathway was stimulated in blocks of 10 minutes alternated by non-stimulated blocks.
994 **(D)** Fat consumption normalized to intake of the first three baseline days for different
995 stimulation frequencies. Plots show fat intake on baseline day3, stimulation day and post-
996 stimulation day. 1Hz stimulation did not change fat consumption (Two-way RM ANOVA, Day x
997 Virus interaction $F(2,72)=1.34$, $p=0.18$). 5Hz stimulation modulated fat intake (Two-way RM
998 ANOVA, Day x Virus interaction, $F(2,72)=3.37$, $p=0.04$) and opsin-expressing mice showed a
999 specific increase in fat intake on stimulation day compared to baseline (Sidák's multiple
1000 comparison test, $p=0.007$). This effect did not extend to 10Hz stimulation (Two-way RM ANOVA,
1001 Day x Virus interaction, $F(2,72)=2.52$, $p=0.09$). **(E)** Video-based analysis of feeding bouts shows
1002 that under control conditions interest in food slowly declines during the hour, but 5Hz
1003 stimulation increases food interactions during later phases of the feeding period (Two-way RM
1004 ANOVA, Interaction Time x Virus, $F(5,110)=2.83$, $p=0.02$, Sidák's multiple comparison test 30-
1005 40m, YFP vs CoChR, $p=0.04$ and 50-60m, $p=0.01$). Mice stimulated with 1Hz displayed a decline
1006 of interest in the fat during the hour and this was not different from control mice (Two-way RM
1007 ANOVA, Interaction Time x Virus, $F(5,120)=0.17$, $p=0.97$). **(F)** Effect of mPFC-LHA stimulation
1008 quantified according to laser ON and OFF blocks. 5Hz stimulation specifically increased fat
1009 interaction during stimulation periods (Two-way RM ANOVA, Interaction Time x Virus,
1010 $F(1,22)=7.64$, $p=0.01$, Sidák's multiple comparison test ON blocks YFP vs CoChR, $p=0.003$). 1Hz
1011 stimulation did not affect feeding bout number (Two-way RM ANOVA, Interaction Time x Virus,
1012 $F(1,24)=0.06$, $p=0.81$). * = $p<0.05$; ** = $p<0.01$.

1013

1014

1015 **Figure 2. mPFC-LHA neuronal activity is diversely modulated by acute social stress**. **(A)** Viral
1016 strategy and implantation of optrodes (i.e. 32 electrode wires and an optic fiber) for
1017 extracellular recordings of identified neurons during social stress. **(B)** Left: Histological
1018 verification of placement of electrode tip in between Channelrhodopsin-expressing mPFC-LHA
1019 neurons. Tip of optrodes indicated with a yellow arrowhead. Right: Histology of LHA targeting
1020 with the Cav2-cre retrograde virus. **(C)** Optogenetic-assisted identification of mPFC pyramidal
1021 neurons projecting to the LHA. Neurons were classified as being light responsive if they showed
1022 a significant increase in firing rate after light stimulation compared to baseline using the SALT-
1023 test. (**D**) Behavioral paradigm to record mPFC-LHA cellular activity during social stress. **(E)** Top:
1024 single cell examples. During the social stress period distinct mPFC-LHA neurons were modulated
1025 in both directions (10s bins comparing 180 seconds right before and after fight onset, Wilcoxon
1026 signed-rank test, $p<0.05$). Bottom: Group averages. Note that the responses outlast the period
1027 of potential physical interaction. Dotted line indicates the average length of the stress exposure.
1028 **(F)** Pie chart showing mPFC-LHA neurons which were significantly modulated by, or not
1029 responsive to, the social stress experience.

1030

1031 **Figure 3. mPFC sends projections to multiple LHA neuronal populations and the mPFC cells**
1032 **responsive to acute hypophagic social stress directly innervate LHA glutamatergic neurons. (A)**
1033 Schematic of the viral strategies to identify LHA populations and to express an opsin in mPFC.
1034 **(B)** Left: Representative image of the viral expression in mPFC (in green) and in LHA cell types (in
1035 red) in coronal slices. Anatomical reference points: fmi forceps minor of the corpus callosum,
1036 EPN entopeduncular nucleus. Right: Representative image of the different LHA neuronal subsets
1037 (red) during patch clamp experiments. **(C)** Experiments to determine synaptic connectivity.
1038 From left to right, cumulative probability plots of opto-evoked AMPAR amplitudes, after mPFC
1039 input stimulation, in LHA_{VGAT} (n cells = 23), LHA_{Vglut2} (n cells = 30), LHA_{MCH} (n cells = 31) and
1040 LHA_{Orexin} (n cells = 37) populations. Alongside are pie chart representations of the proportion of
1041 LHA cells connected to mPFC (n VGAT cells = 27, n Vglut2 cells = 31, n MCH cells = 32 and n
1042 Orexin cells = 38). Trace example within the graph, blue rectangles represent 1 ms of opto-
1043 stimulation. **(D)** Left: Example timeline of EPSCs in an LHA_{VGLUT2} cell during baseline, during
1044 application of TTX and with further addition of 4-AP. Right: Bar graph showing the percentage of
1045 connectivity to mPFC for the 4 LHA populations in presence of 4AP + TTX (n VGAT cells = 10, n
1046 Vglut2 cells = 11, n MCH cells = 9 and n Orexin cells = 12), showing a high monosynaptic
1047 connectivity that was similar across cellular populations (Pearson Chi-Square test, $\chi2=3.166$, $p =$
1048 0.367). **(E)** Schematic and timeline for TRAPing mPFC ensemble during acute stress ($mPFC_{ACUTE}$
1049 $_{STRESS}$) or during novel mouse exposure ($mPFC_{NOVEL\ MOUSE}$). **(F)** Representative image of opsin
1050 expression after TRAP recombination after an acute stress episode in mPFC. (fmi: forceps minor
1051 of the corpus callosum, CPu: caudate-putamen, Prl: prelimbic cortex, IL: infralimbic cortex, DP:
1052 dorsal peduncular cortex). **(G)** Left: Pie charts for connectivity of $mPFC_{ACUTE\ STRESS}$ and $mPFC_{NOVEL}$
1053 $_{MOUSE}$ ensembles with distinct LHA populations (VGAT, Vglut2, MCH and Orexin). Opto-
1054 stimulation of a TRAPed $mPFC_{ACUTE\ STRESS}$ ensemble resulted in more connectivity in
1055 glutamatergic LHA subtypes than LHA_{VGAT} cells ((n VGAT cells = 31, n Vglut2 cells = 49, n MCH
1056 cells = 12 and n Orexin cells = 23, Pearson Chi-Square test, $\chi2=15.783$, $p = 0.001$). Instead,
1057 $mPFC_{NOVEL\ MOUSE}$ ensemble connectivity rates were low with LHA subtypes and did not differ
1058 between them (n VGAT cells = 19, n Vglut2 cells = 8, n MCH cells = 2 and n Orexin cells = 12,
1059 Pearson Chi-Square test, $\chi2=1.187$, $p = 0.756$). Comparing connectivity rates for cell types
1060 between ensembles showed that $mPFC_{ACUTE\ STRESS}$ ensemble connected more to LHA_{VGLUT2} and
1061 LHA_{OREX} neurons than did the $mPFC_{NOVEL\ MOUSE}$ ensemble (LHA_{Vglut2} cells; Pearson Chi-Square
1062 test, $\chi2=4.653$, $p = 0.031$; LHA_{OREX} cells; Pearson Chi-Square test, $\chi2=8.37$, $p = 0.004$). Right:
1063 example of $mPFC_{ACUTE\ STRESS}$ opto-evoked EPSC averaged over sweeps in LHA_{VGAT} (purple),
1064 LHA_{VGLUT2} (blue), LHA_{MCH} (green) and LHA_{OREX} (yellow) neurons. Blue rectangle indicates 1ms
1065 opto-stimulation). * = $p<0.05$; ** = $p<0.01$.

1066

1067

1068 **Figure 4. In the aftermath of social stress, during its hyperphagic phase, specifically the mPFC**
1069 **synapses to LHA_{VGLUT2} neurons are weakened. (A)** Schematic and timeline for patch clamp
1070 electrophysiology in condition of prolonged stress. (**B)** Representative image of opsin expressed
1071 in mPFC and red labeling of the Vglut2 population in the LHA from AAV-DIO-mCherry
1072 recombination, in a Vglut2-cre transgenic line (f: fornix, EPN: entopeduncular nucleus). **(C)**
1073 Cumulative probability of opto-evoked AMPAR amplitude in LHA_{VGLUT2} population, in control
1074 (black) and stress (red), shows a decrease of amplitude after stress (n control = 30, n stress = 35;
1075 Mann-Whitney test, U=342, p = 0.0152). **(D)** Cumulative probability plot for opto-evoked
1076 AMPAR amplitudes at mPFC-LHA_{VGAT} synapses, which are not altered by stress (n control = 23 , n
1077 stress = 21; Mann-Whitney test, U=232, p = 0.8341). **(E)** Cumulative probability plot for opto-
1078 evoked AMPAR amplitudes at mPFC-LHA_{OREX} population (n control = 37 , n stress = 35; Mann-
1079 Whitney test, U=582, p = 0.4663). **(F)** Left: Example traces of mPFC- LHA_{VGLUT2} synaptic
1080 responses during a paired pulse protocol, with 60 ms interpulse interval (IPI) (top), 100 ms
1081 (middle) and 200 ms (bottom). Right: bar graph representation of the paired pulse ratios (PPR)
1082 of mPFC- LHA_{VGLUT2} synapses. Across the 3 IPI protocols there is a significant increase of the PPR
1083 after stress (red), compared to control (black) (n control = 19, n stress = 20; two-way RM
1084 ANOVA, Main effect of group, F(1,37)=4.55, p = 0.04). For C-F data for control cells are as in Fig.
1085 3C. **(G)** Stress does not alter the PPR for mPFC-LHA_{VGAT} synapses (n control = 16, n stress = 18;
1086 two-way RM ANOVA, Main effect of group, F(1,32)=0.160, p = 0.691). **(H)** Stress does not alter
1087 the PPR for mPFC-LHA_{OREX} synapses (n control = 32, n stress = 34; two-way RM ANOVA, Main
1088 effect of group, F(1,64)=1.752, p = 0.19). Blue rectangles represent 1ms opto-stimulation. **(I)**
1089 Schematic and timeline for patch clamp electrophysiological recordings from mPFC-innervated
1090 LHA_{VGLUT2} cells with distinct downstream targets, like Peri-PVN. **(J)** Top left: representative image
1091 of retrograde red tracer targeting of the Peri-PVN. Bottom left: example traces for mPFC-
1092 LHA_{VGLUT2}-Peri-PVN synapses in control (black) and stress (red) conditions during 100 ms paired
1093 pulse protocol. Right: Bar graph representation of the PPR from the three IPIs (n control = 14, n
1094 stress = 12; two-way RM ANOVA, Main effect of group, F(1,24)=5.975, p = 0.022). * = p<0.05.

1095

1096

1097 **Figure 5. *In vivo* mPFC-LHA stimulation further increases fat intake after stress, by preventing**
1098 **a decline of interest in the fat. (A)** Experimental strategy to stimulate mPFC-LHA pathway in
1099 control and stressed conditions. **(B)** Histological verification of mPFC axonal processes in LHA.
1100 Note the dense labeling in LHA, but not in the MH. **(C)** Quantification of fat intake over the 2
1101 hours for experimental groups. Stressed mice consumed more fat than control mice (Two-way
1102 ANOVA, main effect treatment, $F(1,46) = 15$, $p<0.001$) and 5Hz stimulation increased fat (Two-
1103 way ANOVA, main effect stimulation ($F1,46) = 10.38$, $p=0.002$) intake across groups. 5Hz led to a
1104 further increase in fat intake even in stressed mice, making this group the largest consumers of
1105 fat (Sidák's multiple comparison test, $p=0.01$). **(D)** Cumulative plot of feeding bouts for stressed
1106 and control conditions (under mock stimulation) over time. Stressed mice exhibited a binge-like
1107 eating pattern, with over 75% of their feeding bouts occurring within the first 20 minutes (the
1108 Binge phase) with only 25% of further feeding bouts occurring in the subsequent 100 min (Post-
1109 Binge phase). **(E)** Quantification of feeding bouts for non-stimulated mice during the Binge and
1110 Post-binge phase. Stressed mice had significantly more feeding bouts within the first 20 minutes
1111 than controls (Unpaired t-test, $p<0.01$), whereas they interacted less with the fat in the Post-
1112 binge phase than controls (Mann-Whitney test, $p<0.001$). **(F)** 5Hz stimulation did not affect the
1113 number of feeding bouts within the Binge phase (first 20 minutes of the feeding session; Two-
1114 Way ANOVA, interaction Stimulation x Treatment, $F(1,46) = 0.52$, $p=0.48$). **(G)** Instead in the
1115 Post-Binge phase, 5Hz stimulation was more effective in stressed mice than in control mice in
1116 terms of driving further feeding bouts (Two-Way ANOVA, interaction Stimulation x Treatment,
1117 $F(1,46) = 4.05$, $p=0.05$, Sidák's multiple comparison test mock stim vs 5Hz in stressed condition,
1118 $p<0.001$). **(H)** Data in G normalized to total feeding bouts again showing 5Hz stimulation of the
1119 mPFC-LHA in stressed mice drives further fat consumption (Two-Way ANOVA, interaction
1120 Stimulation x Treatment, $F(1,46) = 9.47$, $p=0.004$, Sidák's multiple comparison test Mock stim vs
1121 5Hz in stressed condition, $p<0.001$). * = $p<0.05$; ** = $p<0.01$; *** =$p<0.001$.

1122

1123

1124 **Figure 6. *In vivo* mPFC-LHA chemogenetic inhibition specifically reduces excess fat intake after**
1125 **stress. (A)** Viral strategy to make mPFC-LHA neurons susceptible to chemogenetic inhibition. **(B)**
1126 Histological verification injection sites of CAV2-Cre in the LHA using red beads, and of hM4Di-
1127 mCHerry expression in mPFC (stained against with an antibody for green fluorescence). Note
1128 typical cell distribution of mPFC-LHA neurons in deep layers of the cortex. **(C)** Top: Timeline of
1129 the 2 day social stress experiment driving hyperphagia. Bottom: Delta food intake during test
1130 day (Day +3) compared to a prior baseline session (Day -5). Left: Chemogenetic inhibition of
1131 mPFC-LHA abolished stress-induced overeating of palatable fat, but did not affect food intake
1132 under control conditions (Two-way ANOVA, Treatment x Virus interaction, $F(1,50) = 4.69$,
1133 $p=0.04$, Sidáks multiple comparison test mCherry control vs mCherry Stress, $p=0.02$, hM4Di
1134 control vs hM4Di Stress, $p>0.99$, mCherry control vs hM4Di control, $p=0.61$). Chow intake was
1135 not modulated by stress or by mPFC-LHA inhibition (Two-way ANOVA, Treatment x Virus
1136 interaction, $F(1,50) = 0.07$, $p=0.79$). **(D)** Top: Timeline of the acute social stress experiment
1137 driving transient hypophagia. Acute social stress leads to hypophagia (Two-way ANOVA, main
1138 effect of treatment $F(1,38) = 0.22$, $p<0.001$, Sidák's multiple comparison hM4Di control vs
1139 hM4Di stress, $p=0.007$), but mPFC-LHA inhibition did not abolish this effect (Sidák's multiple
1140 comparison mCherry stress vs hM4Di stress, $p=0.96$). * = $p<0.05$; ** = $p<0.01$.

1141 **References**

1142 1. Oliver, G. & Wardle, J. Perceived effects of stress on food choice. *Physiol Behav* **66**, 511–515
1143 (1999).

1144 2. Adam, T. C. & Epel, E. S. Stress, eating and the reward system. *Physiol Behav* **91**, 449–458 (2007).

1145 3. Linders, L. E. *et al.* Stress-driven potentiation of lateral hypothalamic synapses onto ventral
1146 tegmental area dopamine neurons causes increased consumption of palatable food. *Nat Commun*
1147 **13**, (2022).

1148 4. Dallman, M. F., Pecoraro, N. C. & La Fleur, S. E. Chronic stress and comfort foods: Self-medication
1149 and abdominal obesity. *Brain Behav Immun* **19**, 275–280 (2005).

1150 5. Ulrich-lai, Y. M., Fulton, S., Wilson, M., Petrovich, G. & Rinaman, L. Stress Exposure, Food Intake,
1151 and Emotional State. **18**, 381–399 (2016).

1152 6. Arnsten, A. F. T. Stress signalling pathways that impair prefrontal cortex structure and function.
1153 *Nat Rev Neurosci* **10**, 410–22 (2009).

1154 7. Vander Weele, C. M., Siciliano, C. A. & Tye, K. M. Dopamine tunes prefrontal outputs to
1155 orchestrate aversive processing. *Brain Research* Preprint at
1156 https://doi.org/10.1016/j.brainres.2018.11.044 (2019).

1157 8. Balodis, I. M., Grilo, C. M. & Potenza, M. N. Neurobiological features of binge eating disorder. *CNS*
1158 *Spectrums* vol. 20 557–565 Preprint at https://doi.org/10.1017/S1092852915000814 (2015).

1159 9. Val-Laillet, D. *et al.* Neuroimaging and neuromodulation approaches to study eating behavior and
1160 prevent and treat eating disorders and obesity. *Neuroimage Clin* **8**, 1–31 (2015).

1161 10. Land, B. B. *et al.* Medial prefrontal D1 dopamine neurons control food intake. *Nat Neurosci* **17**,
1162 248–53 (2014).

1163 11. Mena, J. D., Selleck, R. A. & Baldo, B. A. Mu-Opioid Stimulation in Rat Prefrontal Cortex Engages
1164 Hypothalamic Orexin / Hypocretin-Containing Neurons , and Reveals Dissociable Roles of Nucleus
1165 Accumbens and Hypothalamus in Cortically Driven Feeding. *The Journal of Neuroscience* **33**,
1166 18540–18552 (2013).

1167 12. Reppucci, C. J. & Petrovich, G. D. Organization of connections between the amygdala, medial
1168 prefrontal cortex, and lateral hypothalamus: a single and double retrograde tracing study in rats.
1169 *Brain Struct Funct* **221**, 2937–2962 (2016).

1170 13. Stuber, G. D. & Wise, R. A. Lateral hypothalamic circuits for feeding and reward. *Nat Neurosci* **19**,
1171 198–205 (2016).

1172 14. Bonnavion, P., Mickelsen, L. E., Fujita, A., de Lecea, L. & Jackson, A. C. Hubs and spokes of the
1173 lateral hypothalamus: cell types, circuits and behaviour. *Journal of Physiology* **594**, 6443–6462
1174 (2016).

1175 15. Rossi, M. A. Control of energy homeostasis by the lateral hypothalamic area. *Trends in*
1176 *Neurosciences* Preprint at https://doi.org/10.1016/j.tins.2023.05.010 (2023).

1177 16. Berthoud, H. R. & Münzberg, H. The lateral hypothalamus as integrator of metabolic and
1178 environmental needs: From electrical self-stimulation to opto-genetics. *Physiol Behav* **104**, 29–39
1179 (2011).

1180 17. Stuber, G. D. Neurocircuits for motivation. *Science (1979)* (2023).

1181 18. Mickelsen, L. E. *et al.* Single-cell transcriptomic analysis of the lateral hypothalamic area reveals
1182 molecularly distinct populations of inhibitory and excitatory neurons. *Nat Neurosci* **22**, 642–656
1183 (2019).

1184 19. Barbano, M. F., Wang, H.-L., Morales, M. & Wise, R. A. Feeding and Reward Are Differentially
1185 Induced by Activating GABAergic Lateral Hypothalamic Projections to VTA. *The Journal of*
1186 *Neuroscience* **36**, 2975–2985 (2016).

1187 20. Padilla-Coreano, N. *et al.* Cortical ensembles orchestrate social competition through hypothalamic
1188 outputs. *Nature* **603**, 667–671 (2022).

1189 21. Clarke, R. E. *et al.* Identification of a Stress-Sensitive Anorexigenic Neurocircuit From Medial
1190 Prefrontal Cortex to Lateral Hypothalamus. *Biol Psychiatry* **93**, 309–321 (2023).

1191 22. Benchenane, K., Tiesinga, P. H. & Battaglia, F. P. Oscillations in the prefrontal cortex: A gateway to
1192 memory and attention. *Current Opinion in Neurobiology* vol. 21 475–485 Preprint at
1193 https://doi.org/10.1016/j.conb.2011.01.004 (2011).

1194 23. Yau, Y. H. C. & Potenza, M. N. Stress and eating behaviors. *Minerva Endocrinol* **38**, 255–267
1195 (2013).

1196 24. Razzoli, M., Sanghez, V. & Bartolomucci, A. Chronic Subordination Stress Induces Hyperphagia and
1197 Disrupts Eating Behavior in Mice Modeling Binge-Eating-Like Disorder. *Front Nutr* **1**, (2015).

1198 25. Linders, L. E. *et al.* Studying Synaptic Connectivity and Strength with Optogenetics and Patch-
1199 Clamp Electrophysiology. *International Journal of Molecular Sciences* vol. 23 Preprint at
1200 https://doi.org/10.3390/ijms231911612 (2022).

1201 26. Petreanu, L., Huber, D., Sobczyk, A. & Svoboda, K. Channelrhodopsin-2-assisted circuit mapping of
1202 long-range callosal projections. *Nat Neurosci* **10**, 663–668 (2007).

1203 27. Kakava-Georgiadou, N. *et al.* An intersectional approach to target neural circuits with cell- and
1204 projection-type specificity: Validation in the mesolimbic dopamine system. *Front Mol Neurosci*
1205 (2019) doi:10.3389/fnmol.2019.00049.

1206 28. Petreanu, L., Mao, T., Sternson, S. M. & Svoboda, K. The subcellular organization of neocortical
1207 excitatory connections. *Nature* **457**, 1142–1145 (2009).

1208 29. DeNardo, L. A. *et al.* Temporal evolution of cortical ensembles promoting remote memory
1209 retrieval. *Nat Neurosci* **22**, 460–469 (2019).

1210 30. Koutlas, I. *et al.* Characterizing and TRAPing a Social Stress-Activated Neuronal Ensemble in the
1211 Ventral Tegmental Area. *Front Behav Neurosci* **16**, (2022).

1212 31. Biro, L. *et al.* Task division within the prefrontal cortex: Distinct neuron populations selectively
1213 control different aspects of aggressive behavior via the hypothalamus. *Journal of Neuroscience*
1214 **38**, 4065–4075 (2018).

1215 32. Rossi, M. A. *et al.* Transcriptional and functional divergence in lateral hypothalamic glutamate
1216 neurons projecting to the lateral habenula and ventral tegmental area. *Neuron* (2021)
1217 doi:10.1016/j.neuron.2021.09.020.

1218 33. Stamatakis, A. M. *et al.* Lateral Hypothalamic Area Glutamatergic Neurons and Their Projections
1219 to the Lateral Habenula Regulate Feeding and Reward. *Journal of Neuroscience* **36**, 302–311
1220 (2016).

1221 34. Herman, J. P., Tasker, J. G., Ziegler, D. R. & Cullinan, W. E. Local circuit regulation of
1222 paraventricular nucleus stress integration. *Pharmacol Biochem Behav* **71**, 457–468 (2002).

1223 35. Chen, L. *et al.* Glutamatergic lateral hypothalamus promotes defensive behaviors.
1224 *Neuropharmacology* **178**, (2020).

1225 36. Berrios, J. *et al.* Food cue regulation of AGRP hunger neurons guides learning. *Nature* **595**, 695–
1226 700 (2021).

1227 37. Nieh, E. H. *et al.* Inhibitory Input from the Lateral Hypothalamus to the Ventral Tegmental Area
1228 Disinhibits Dopamine Neurons and Promotes Behavioral Activation. *Neuron* **90**, 1286–1298
1229 (2016).

1230 38. Nieh, E. H. *et al.* Decoding neural circuits that control compulsive sucrose seeking. *Cell* **160**, 528–
1231 541 (2015).

1232 39. Zingg, B. *et al.* AAV-Mediated Anterograde Transsynaptic Tagging: Mapping Corticocollicular
1233 Input-Defined Neural Pathways for Defense Behaviors. *Neuron* **93**, 33–47 (2017).

1234 40. Dallman, M. F. Stress-induced obesity and the emotional nervous system. *Trends in Endocrinology*
1235 *and Metabolism* **21**, 159–165 (2010).

1236 41. Chen, C. *et al.* The dynamic state of a prefrontal–hypothalamic–midbrain circuit commands
1237 behavioral transitions. *Nat Neurosci* (2024) doi:10.1038/s41593-024-01598-3.

1238 42. Noritake, A., Ninomiya, T., Kobayashi, K. & Isoda, M. Chemogenetic dissection of a prefrontal-
1239 hypothalamic circuit for socially subjective reward valuation in macaques. *Nat Commun* **14**,
1240 (2023).

1241 43. Rossi, M. A. *et al.* Obesity remodels activity and transcriptional state of a lateral hypothalamic
1242 brake on feeding. *Science (1979)* **364**, 1271–1274 (2019).

1243 44. Sternson, S. M. & Eiselt, A. K. Three Pillars for the Neural Control of Appetite. *Annual Review of*
1244 *Physiology* vol. 79 401–423 Preprint at https://doi.org/10.1146/annurev-physiol-021115-104948
1245 (2017).

1246 45. Zupančič, M. *et al.* Brain-wide mapping of efferent projections of glutamatergic (Onecut3 $^{+}$)
1247 neurons in the lateral mouse hypothalamus. *Acta Physiologica* **238**, (2023).

1248 46. Vong, L. *et al.* Leptin Action on GABAergic Neurons Prevents Obesity and Reduces Inhibitory Tone
1249 to POMC Neurons. *Neuron* **71**, 142–154 (2011).

1250 47. Voigts, J., Siegle, J. H., Pritchett, D. L. & Moore, C. I. The flexDrive: an ultra-light implant for optical
1251 control and highly parallel chronic recording of neuronal ensembles in freely moving mice. *Front*
1252 *Syst Neurosci* **7**, (2013).

1253 48. Siegle, J. H. *et al.* Open Ephys: an open-source, plugin-based platform for multichannel
1254 electrophysiology. *J Neural Eng* **14**, 045003 (2017).

1255 49. Ludwig, K. A. *et al.* Using a Common Average Reference to Improve Cortical Neuron Recordings
1256 From Microelectrode Arrays. *J Neurophysiol* **101**, 1679–1689 (2009).

1257 50. Kvitsiani, D. *et al.* Distinct behavioural and network correlates of two interneuron types in
1258 prefrontal cortex. *Nature* **498**, 363–366 (2013).

1259 51. Schmitzer-Torbert, N., Jackson, J., Henze, D., Harris, K. & Redish, A. D. Quantitative measures of
1260 cluster quality for use in extracellular recordings. *Neuroscience* **131**, 1–11 (2005).

1261 52. Terra, H. *et al.* Prefrontal Cortical Projection Neurons Targeting Dorsomedial Striatum Control
1262 Behavioral Inhibition. *Current Biology* **30**, 4188-4200.e5 (2020).

1263 53. Burgos-Robles, A. *et al.* Amygdala inputs to prefrontal cortex guide behavior amid conflicting cues
1264 of reward and punishment. *Nat Neurosci* **20**, 824–835 (2017).

1265

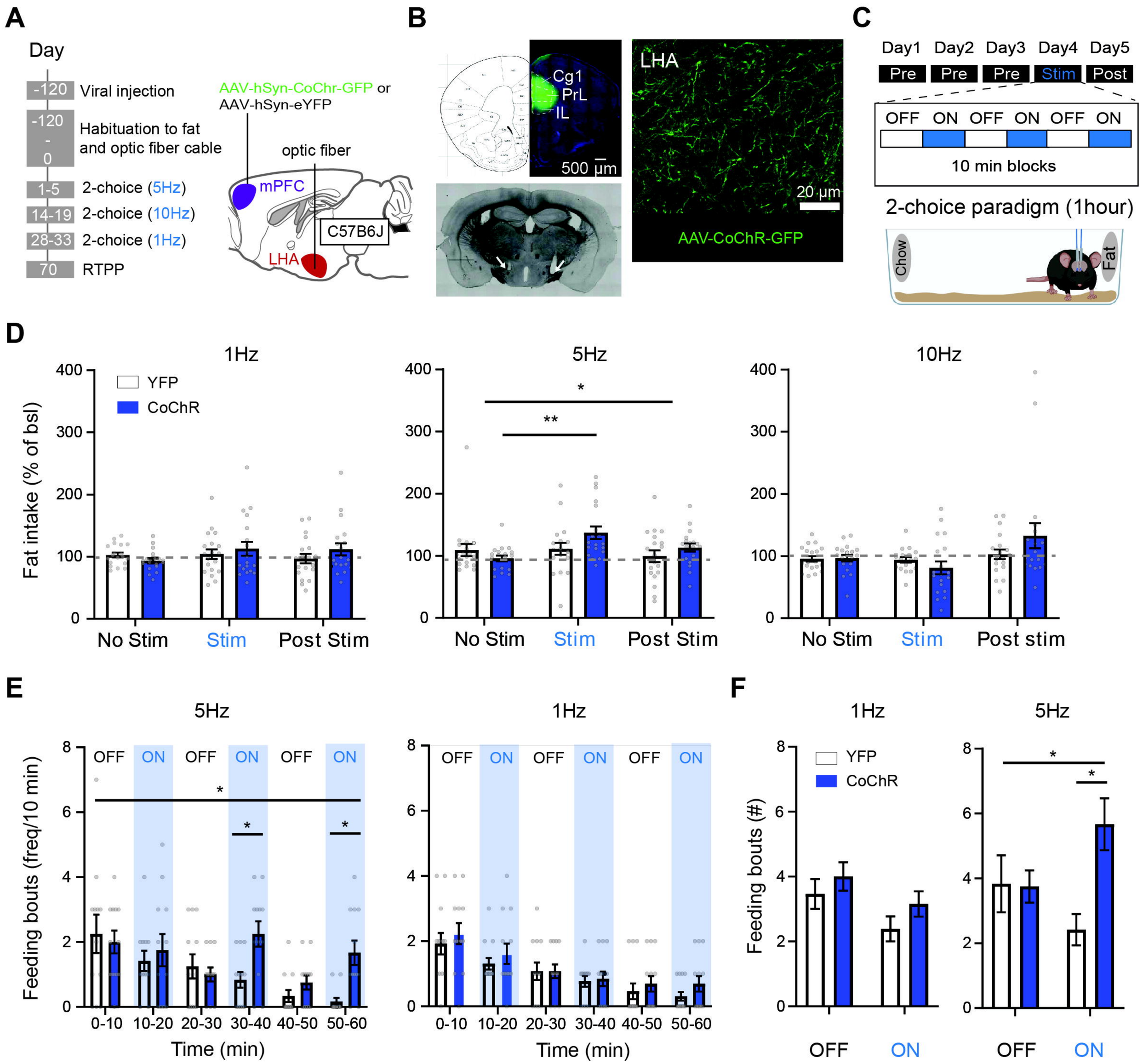
A
Day
-120 Viral injection
-120 - 0 Habituation to fat and optic fiber cable
1-5 2-choice (5Hz)
14-19 2-choice (10Hz)
28-33 2-choice (1Hz)
70 RTPP
AAV-hSyn-CoChr-GFP or AAV-hSyn-eYFP
optic fiber
mPFC
C57B6J
LHA
B
Cg1
PrL
IL
500 µm
LHA
20 µm
AAV-CoChR-GFP
C
Day1 Day2 Day3 Day4 Day5
Pre Pre Pre Stim Post
OFF ON OFF ON OFF ON
10 min blocks
2-choice paradigm (1hour)
Chow
Fat
D
1Hz
5Hz
10Hz
YFP
CoChR
Fat intake (% of bsl)
No Stim
Stim
Post Stim
Post stim
E
5Hz
1Hz
Feeding bouts (freq/10 min)
OFF ON OFF ON OFF ON
0-10 10-20 20-30 30-40 40-50 50-60
Time (min)
F
1Hz
5Hz
Feeding bouts (#)
OFF
ON

Figure 1

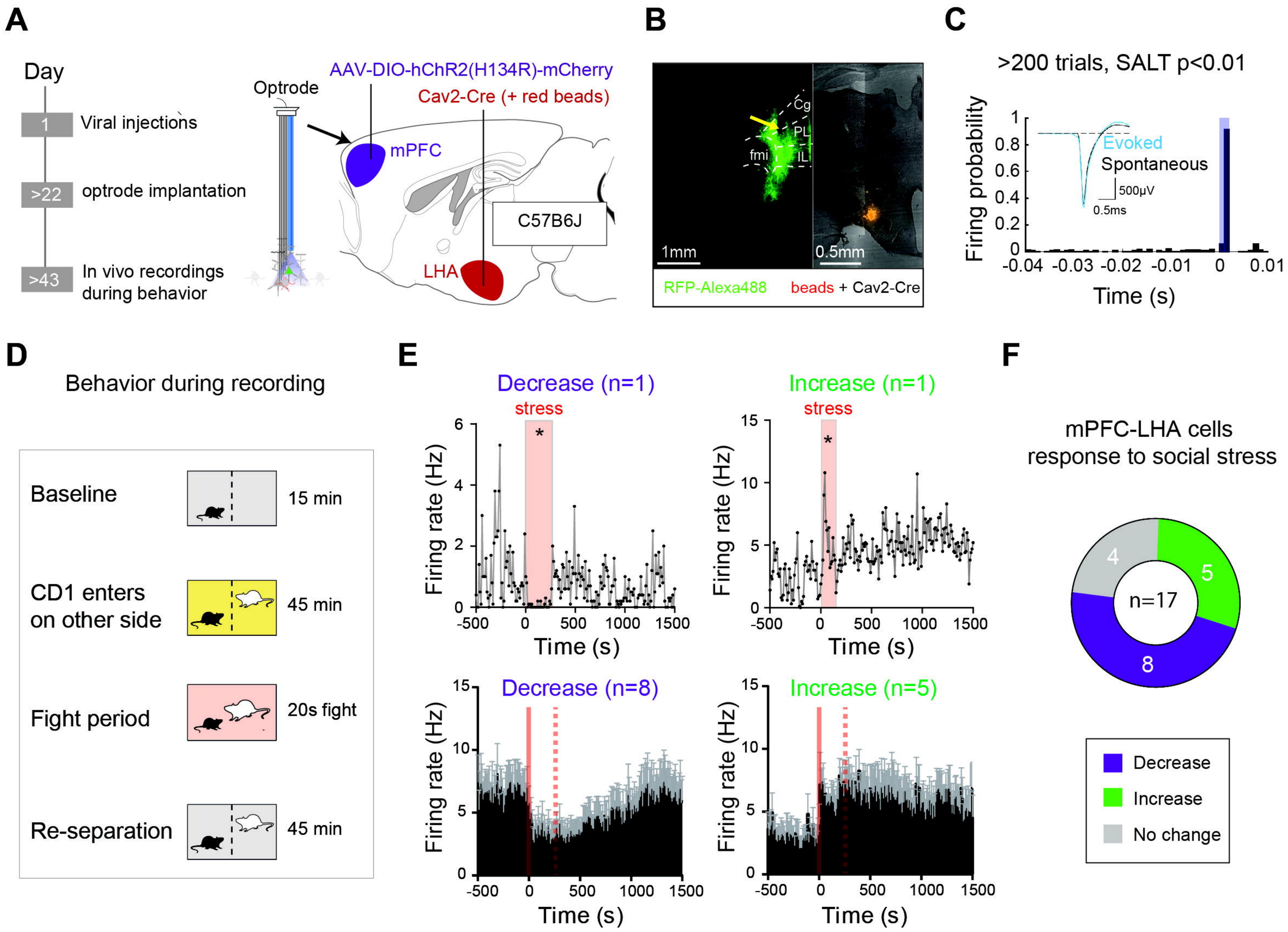
A
Day
1
Viral injections
>22
optrode implantation
>43
In vivo recordings during behavior
Optrode
AAV-DIO-hChR2(H134R)-mCherry
Cav2-Cre (+ red beads)
mPFC
C57B6J
LHA
B
Cg
PL
fmi
IL
1mm
0.5mm
RFP-Alexa488
beads + Cav2-Cre
C
>200 trials, SALT p<0.01
Firing probability
Evoked
Spontaneous
500µV
0.5ms
Time (s)
D
Behavior during recording
Baseline
15 min
CD1 enters on other side
45 min
Fight period
20s fight
Re-separation
45 min
E
Decrease (n=1)
Increase (n=1)
stress
Firing rate (Hz)
Time (s)
Decrease (n=8)
Increase (n=5)
F
mPFC-LHA cells response to social stress
n=17
4
5
8
Decrease
Increase
No change

Figure 2

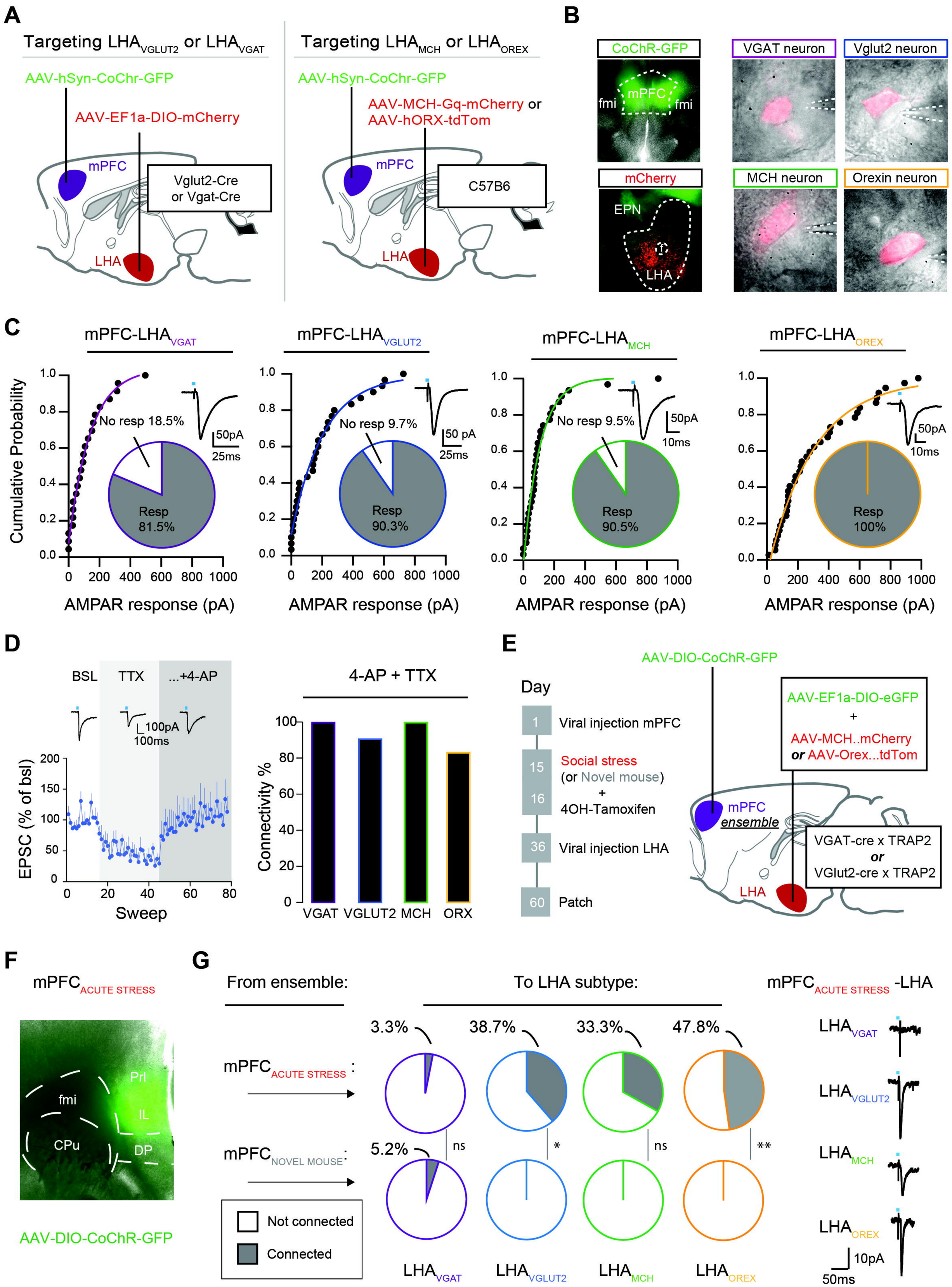
A
Targeting LHA VGLUT2 or LHA VGAT
AAV-hSyn-CoChr-GFP
AAV-EF1a-DIO-mCherry
mPFC
Vglut2-Cre
or Vgat-Cre
LHA
Targeting LHA MCH or LHA OREX
AAV-hSyn-CoChr-GFP
AAV-MCH-Gq-mCherry or
AAV-hORX-tdTom
mPFC
C57B6
LHA
B
CoChR-GFP
fmi
mPFC
fmi
VGAT neuron
Vglut2 neuron
mCherry
EPN
LHA
MCH neuron
Orexin neuron
C
mPFC-LHA VGAT
mPFC-LHA VGLUT2
mPFC-LHA MCH
mPFC-LHA OREX
Cumulative Probability
No resp 18.5%
50pA
25ms
Resp
81.5%
No resp 9.7%
50 pA
25ms
Resp
90.3%
No resp 9.5%
50pA
10ms
Resp
90.5%
50pA
10ms
Resp
100%
AMPAR response (pA)
D
BSL
TTX
...+4-AP
100pA
100ms
EPSC (% of bsl)
Sweep
4-AP + TTX
Connectivity %
VGAT
VGLUT2
MCH
ORX
E
Day
1 Viral injection mPFC
15 Social stress
(or Novel mouse)
+
16 4OH-Tamoxifen
36 Viral injection LHA
60 Patch
AAV-DIO-CoChR-GFP
AAV-EF1a-DIO-eGFP
+
AAV-MCH..mCherry
or AAV-Orex...tdTom
mPFC
ensemble
VGAT-cre x TRAP2
or
VGlut2-cre x TRAP2
LHA
F
mPFC ACUTE STRESS
Prl
fmi
IL
CPu
DP
AAV-DIO-CoChR-GFP
G
From ensemble:
To LHA subtype:
mPFC ACUTE STRESS -LHA
3.3%
38.7%
33.3%
47.8%
mPFC ACUTE STRESS :
mPFC NOVEL MOUSE:
5.2%
ns
*
ns
**
Not connected
Connected
LHA VGAT
LHA VGLUT2
LHA MCH
LHA OREX
10pA
50ms

Figure 3

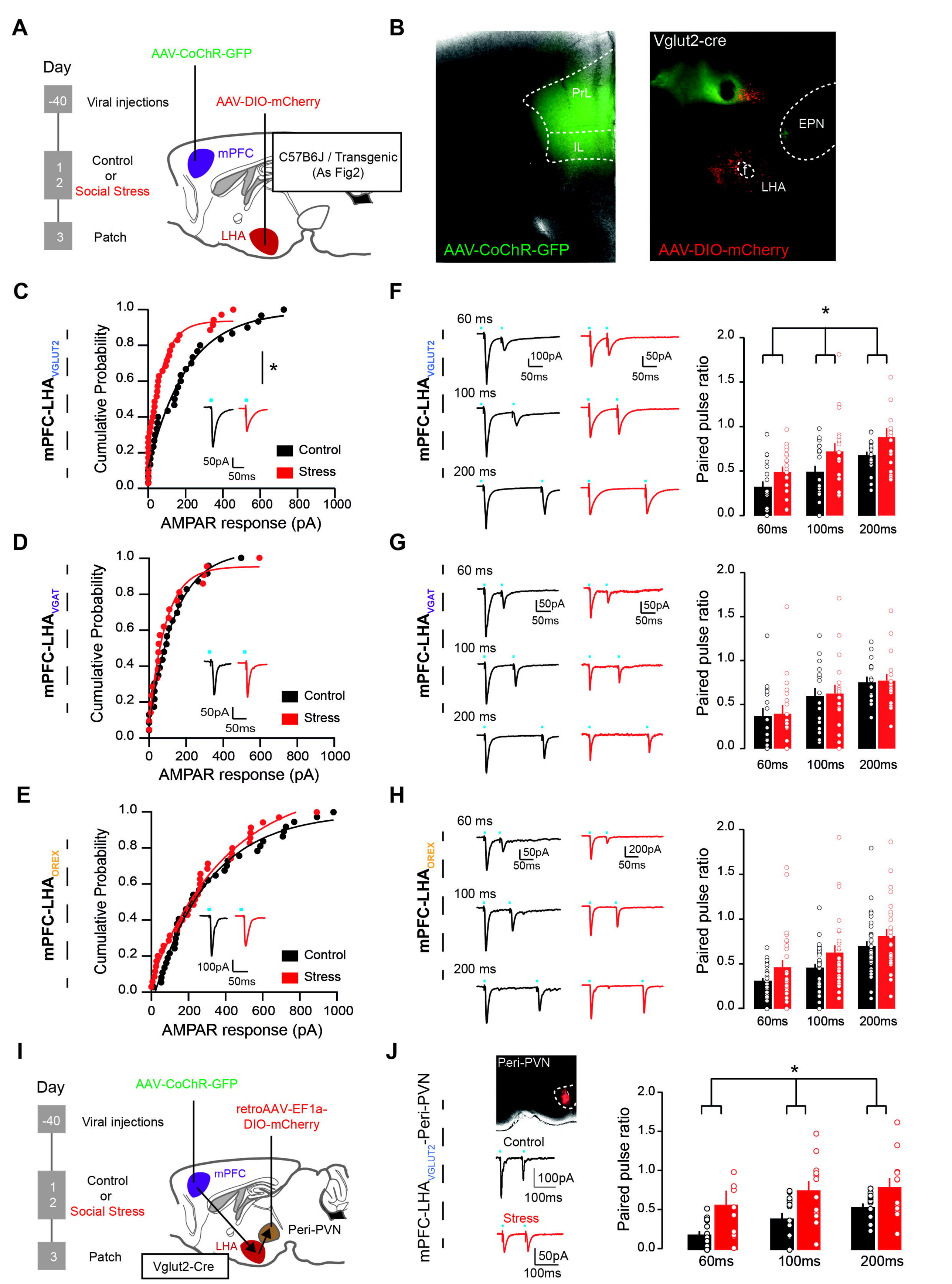
A
Day
-40
Viral injections
AAV-CoChR-GFP
AAV-DIO-mCherry
1
2
Control
or
Social Stress
3
Patch
mPFC
LHA
C57B6J / Transgenic
(As Fig2)
B
PrL
IL
AAV-CoChR-GFP
Vglut2-cre
EPN
LHA
AAV-DIO-mCherry
C
mPFC-LHA VGLUT2
Cumulative Probability
AMPAR response (pA)
50pA
50ms
Control
Stress
D
mPFC-LHA VGAT
E
mPFC-LHA OREX
100pA
F
60 ms
100 ms
200 ms
100pA
Paired pulse ratio
60ms
100ms
200ms
G
H
I
AAV-CoChR-GFP
retroAAV-EF1a-
DIO-mCherry
mPFC
Peri-PVN
Vglut2-Cre
J
mPFC-LHA VGLUT2-Peri-PVN
Peri-PVN
Control
Stress

Figure 4

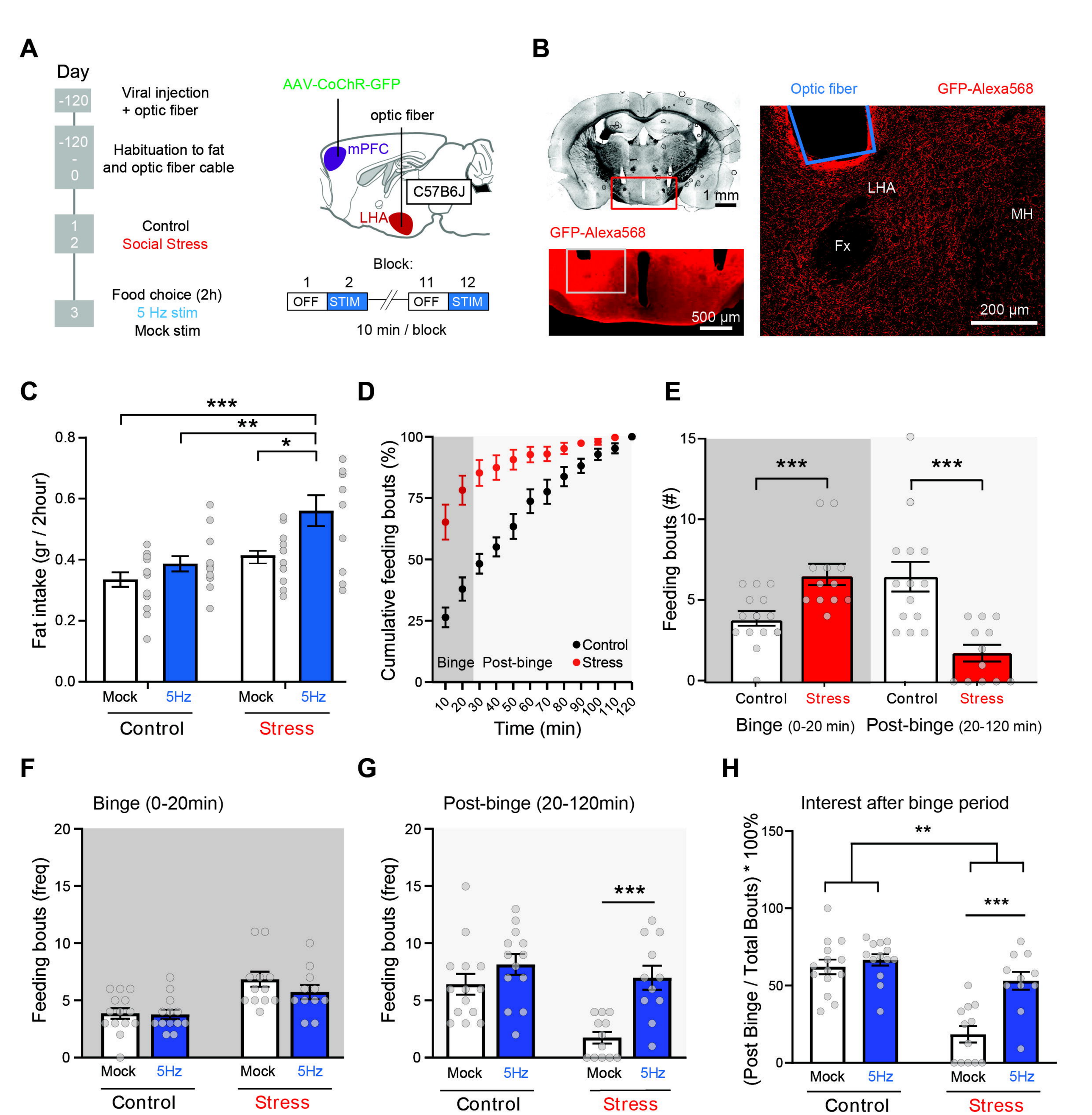
A
Day
-120
Viral injection
+ optic fiber
-120
-
0
Habituation to fat
and optic fiber cable
1
2
Control
Social Stress
3
Food choice (2h)
5 Hz stim
Mock stim
AAV-CoChR-GFP
optic fiber
mPFC
C57B6J
LHA
Block:
1
2
11
12
OFF
STIM
OFF
STIM
10 min / block
B
1 mm
GFP-Alexa568
500 µm
Optic fiber
GFP-Alexa568
LHA
MH
Fx
200 µm
C
***
**
*
Fat intake (gr / 2hour)
0.0
0.2
0.4
0.6
0.8
Mock
5Hz
Mock
5Hz
Control
Stress
D
Cumulative feeding bouts (%)
0
25
50
75
100
Binge
Post-binge
Control
Stress
10
20
30
40
50
60
70
80
90
100
110
120
Time (min)
E
Feeding bouts (#)
0
5
10
15
***
***
Control
Stress
Control
Stress
Binge (0-20 min)
Post-binge (20-120 min)
F
Binge (0-20min)
Feeding bouts (freq)
0
5
10
15
20
Mock
5Hz
Mock
5Hz
Control
Stress
G
Post-binge (20-120min)
Feeding bouts (freq)
0
5
10
15
20
***
Mock
5Hz
Mock
5Hz
Control
Stress
H
Interest after binge period
(Post Binge / Total Bouts) * 100%
0
50
100
150
**
***
Mock
5Hz
Mock
5Hz
Control
Stress

Figure 5

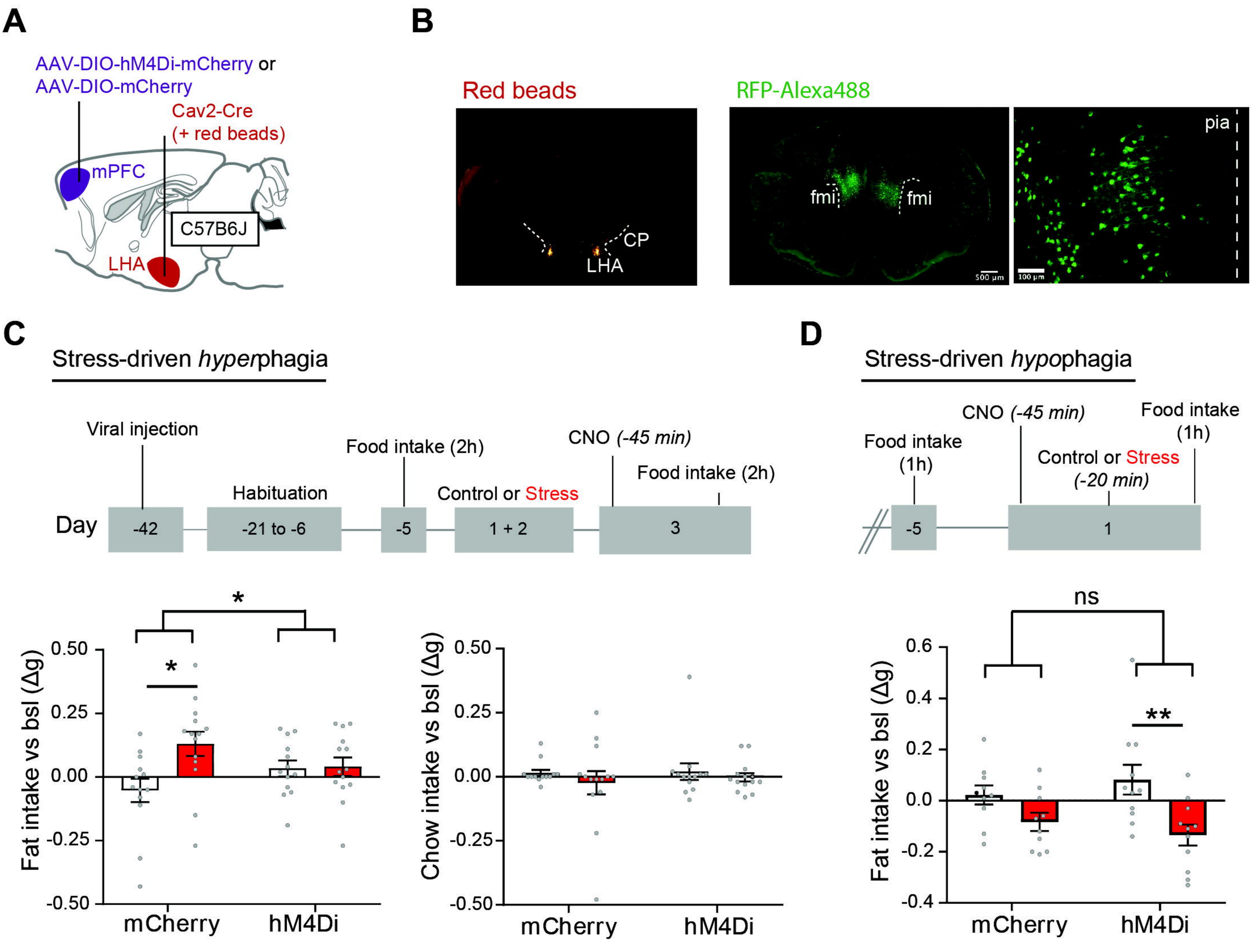
A
AAV-DIO-hM4Di-mCherry or
AAV-DIO-mCherry
Cav2-Cre
(+ red beads)
mPFC
C57B6J
LHA
B
Red beads
RFP-Alexa488
CP
LHA
fmi
fmi
pia
500 µm
100 µm
C
Stress-driven hyperphagia
Viral injection
Habituation
Food intake (2h)
Control or Stress
CNO (-45 min)
Food intake (2h)
Day
-42
-21 to -6
-5
1 + 2
3
Fat intake vs bsl (Δg)
Chow intake vs bsl (Δg)
mCherry
hM4Di
D
Stress-driven hypophagia
Food intake
(1h)
CNO (-45 min)
Control or Stress
(-20 min)
Food intake
(1h)
-5
1
ns
**
Fat intake vs bsl (Δg)
mCherry
hM4Di

Figure 6